Neutron scattering/Diffusion de neutrons

Neutrons probing the structure and dynamics of liquids

Françoise Leclercq-Hugeux [a,*], Marie-Vanessa Coulet [b], Jean-Pierre Gaspard [c],
Stéphanie Pouget [d], Jean-Marc Zanotti [e]

[a] *LASIR/HEI, UMR 8516 CNRS, 13, rue de Toul, 59046 Lille, France*
[b] *Laboratoire TECSEN – UMR 6122 CNRS Université Paul-Cézanne, 13397 Marseille cedex 20, France*
[c] *University of Liège, B5, B-4000 Sart-Tilman, Belgium*
[d] *Service général des rayons X – DRFMC/SP2M, CEA, 38042 Grenoble cedex, France*
[e] *Laboratoire Léon-Brillouin (CEA–CNRS), CEA Saclay, 91191 Gif-sur-Yvette cedex, France*

Available online 26 November 2007

Abstract

This article illustrates the benefits of neutron techniques to the understanding of the liquid state. As opposed to the nearly complete order of crystals or the nearly complete disorder of gases, a liquid's disorder is partial and results from dynamical events acting on a broad range of space and time scales. Consequently, no single, simple parameter can encompass the concept of order or disorder in the liquid state. The wide variety of neutron techniques (diffraction, quasi-elastic and inelastic scattering) is a key asset to solve the issue. Selected studies ranging over typical interactions and conditions relevant to liquids (metallic, covalent, molecular, liquids near a phase transition and confined fluids) are presented. In each case, both structural and dynamical aspects, along with the connections to complementary techniques (computer simulation, X-ray absorption and/or scattering) are highlighted. ***To cite this article: F. Leclercq-Hugeux et al., C. R. Physique 8 (2007).***
© 2007 Académie des sciences. Published by Elsevier Masson SAS. All rights reserved.

Résumé

Les neutrons sondent la structure et la dynamique des liquides. Cet article illustre l'apport des méthodes neutroniques à la compréhension de l'état liquide. A la différence du cristal qui présente un ordre presque parfait et du gaz où les particules sont presque indépendantes les unes des autres, le désordre de l'état liquide est partiel et résulte de processus dynamiques intervenant sur des grandes échelles de distances et de temps caractéristiques. En conséquence il n'existe pas de paramètre simple et unique permettant de décrire l'ordre ou le désordre des liquides. La palette des techniques instrumentales de diffusion de neutrons est variée (diffraction, diffusion diffuse, diffusion quasi-élastique et inélastique) et particulièrement bien adaptée pour apporter des éclairages focalisés sur la nature de ce désordre. Nous présentons ici des exemples caractéristiques de types d'interactions différentes ou d'états thermodynamiques typiques de l'état liquide (liquides métalliques, covalents, moléculaires, liquides à l'approche d'une transition de phase, fluides confinés). Pour chacune de ces illustrations nous tenterons d'aborder à la fois les aspects structuraux et dynamiques en relation avec des approches complémentaires utilisant le rayonnement synchrotron (diffraction ou spectroscopies d'absorption) ou les méthodes numériques. ***Pour citer cet article : F. Leclercq-Hugeux et al., C. R. Physique 8 (2007).***
© 2007 Académie des sciences. Published by Elsevier Masson SAS. All rights reserved.

Keywords: Neutron scattering; Liquid state

* Corresponding author.
E-mail addresses: francoise.leclercq@hei.fr (F. Leclercq-Hugeux), vanessa.coulet@univ-cezanne.fr (M.-V. Coulet), jp.gaspard@ulg.ac.be (J.-P. Gaspard), spouget@cea.fr (S. Pouget), jean-marc.zanotti@cea.fr (J.-M. Zanotti).

1. Introduction

Liquids are ubiquitous materials in the everyday world. They are important in many fields of science: physics, chemistry, life sciences and earth sciences. The liquid state is intermediate between the crystalline state characterized by a long range order (LRO) (the crystallographic unit cell repeated to infinity for a perfect crystal), and the gas state in which atoms or molecules have random atomic positions. The liquid state extends over a wide density range from the melting point (dense liquid) up to the liquid–vapour critical point (supercritical fluid).

The structure of condensed matter (solid and liquid) is driven by the electrostatic interactions and the electron delocalization imposed by quantum physics. The interatomic interactions are responsible for a local or short-range order (SRO). Upon melting, the long range translational order (LRO) characterizing the crystalline solid (which gives rise to Bragg peaks in the scattering pattern) is reduced to SRO over a few intermolecular distances. As atoms (or molecules) vibrate and diffuse in the liquid, the atomic positions are disordered and then the liquid state requires statistical descriptions: the averaged structure is given by the spatial correlations of the atomic positions. The pair distribution function $g(r)$ characterizes the modulation of the local density $\rho(r)$ around a given atom as a function of the distance r from that atom. Information concerning the dynamics of the system can be deduced from the time dependent correlation function $G(r, t)$ which gives the probability of finding an atom at position r, at time t, knowing that a given atom was at position r_0 at time t_0.

Neutron scattering techniques are well suited to the study of liquid disorder. The neutrons are scattered by the nuclei (strong interactions) and also, weakly, by magnetic fields including those due to magnetic moments of unpaired electrons. Their wavelength and energy can be chosen to match the characteristic distances and energies at play in condensed matter. Thermal neutrons ($T = 300$ K) have an associated wavelength of the order of 1.8 Å and an energy of 25 meV (typical of vibrational energies). They give access to the order prevailing in liquids for distances extending from about 1 Å (typically characteristic for the short range interatomic order) up to a few thousands of Å (large molecular entities, aggregates, micelles and clusters). For a complete understanding and characterization of a specific liquid it is essential to investigate the dynamics at these different characteristic distances i.e. at different relaxation times: intramolecular motions ($\tau \approx 10^{-14}$ s: vibrations, torsional motions around intramolecular bonds); molecular motion as a whole ($\tau \approx 10^{-12}$ s) for translational diffusion and rotation around molecular axes, dynamics of mesoscopic particles at larger time scale.

The aim of this paper is not to provide an exhaustive review of the works performed on liquid systems. An extensive presentation of the liquid state, discussing in detail how liquid properties, macroscopic or microscopic, are related to the details of the atomic motions or the atomic positions is given in the reference book from P.A. Egelstaff [1]. Let us note that in this book, special attention is given to a general overview of the available measuring techniques and the significance of the results obtained. Neutron and X-ray diffraction studies of liquids and glasses were recently reviewed by Fischer et al. [2]. This widely referenced review emphasizes the instrumental approach and data analysis methods as well as recent progress in computer simulations. Finally, we would like to mention the paper from P. Chieux reviewing the structure determination of disordered materials by neutron scattering from simple to complex systems [3].

Our objective is to illustrate the contribution of neutron techniques to the understanding of the liquid state. We have selected several recent studies dealing with different kinds of interactions (metallic, covalent, molecular) and different conditions (liquids near a phase transition and confined liquids), focusing on both structural and dynamical aspects.

After an overview of the theoretical formalism of neutron scattering by liquids, the complementarities with other experimental methods and computer simulations are discussed in Section 2. Section 3 is devoted to structural studies in liquid metals and liquid semiconductors. Then, the powerful advantage of neutron techniques to give access to both structure and dynamics of the liquid state, probing different characteristic lengths and relaxation times is emphasized. Section 4 gives some examples of analysis of the structure factor of molecular liquids focusing on the separation of intra and inter contributions. Section 5 treats the mesoscopic behaviour of fluids near the liquid-gas critical point. Finally, Section 6 addresses the influence of the confinement on the structure and the dynamics of a liquid.

2. Neutron scattering by liquids

2.1. Formalism

The double differential neutron scattering cross-section, which describes the scattering by a sample of a neutron beam with incident wave vector $\mathbf{k}_0$ and a final wave vector $\mathbf{k}$, in the solid angle $d\Omega$, is directly related to the dynamic structure factor $S(\mathbf{Q}, \omega)$

$$\frac{d^2\sigma}{d\Omega\,d\omega} = \frac{k}{k_0}\langle b^2\rangle S(\mathbf{Q}, \omega) + A\delta(\mathbf{Q}) \tag{1}$$

where the amplitude factor $\langle b^2\rangle$ is characteristic of the average neutron interaction with the different scattering centres (b is the scattering length of a given nucleus in the Fermi pseudo potential approximation). The momentum and energy transfers are respectively defined as $\mathbf{Q} = \mathbf{k}_0 - \mathbf{k}$ and $\omega = \hbar(k_0^2 - k^2)/2m$, m being the neutron mass. The factor k/k_0 corresponds to the conversion of neutron density to neutron flux. $A\delta(\mathbf{Q})$ sums up different $Q = 0$ terms.

The dynamic structure factor $S(\mathbf{Q}, \omega)$ is the Fourier transform of the time dependent correlation function $G(\mathbf{r}, t)$:

$$S(\mathbf{Q}, \omega) = \frac{1}{2\pi} \int_V \int_{-\infty}^{\infty} \exp[i\mathbf{Q}.\mathbf{r} - \omega t]\big[G(\mathbf{r}, t) - \rho\big]\,d\mathbf{r}\,dt \tag{2}$$

where ρ is the average particle density.

To get some insight into the characteristics of the scattering function $S(\mathbf{Q}, \omega)$ in different $\mathbf{Q}$ and ω ranges, it is convenient to distinguish in $G(\mathbf{r}, t)$ a self-contribution $G_s(\mathbf{r}, t)$ which correlates the positions of a given particle at two successive times. The differential neutron scattering cross-section is then split into two contributions: the coherent scattering characteristic of collective behaviour and the incoherent scattering resulting from self correlations. The coherent part deals with the position correlation of two atoms (distinct or not) and depends on the coherent cross-section $\sigma_{coh} = 4\pi\langle b\rangle^2$ with $\langle b\rangle$ the average scattering length, whereas the incoherent term is weighted by the variance of the scattering lengths $\sigma_{incoh} = 4\pi(\langle b^2\rangle - \langle b\rangle^2)$.

$$\frac{d^2\sigma}{d\Omega\,d\omega} = \left(\frac{d^2\sigma}{d\Omega\,d\omega}\right)_{coh} + \left(\frac{d^2\sigma}{d\Omega\,d\omega}\right)_{incoh} = \frac{k}{k_0}\big[\langle b\rangle^2 S(\mathbf{Q}, \omega) + (\langle b^2\rangle - \langle b\rangle^2)S_{incoh}(\mathbf{Q}, \omega)\big] + A\delta(\mathbf{Q}) \tag{3}$$

Fig. 1 gives a sketch of the qualitative behaviour of $S(Q, \omega)$ in case of an isotropic compressible fluid. The limit at $Q = 0$ relates the microscopic description given by correlation functions to the macroscopic isothermal compressibility. At low Q ($Q < 1$ Å^{-1}) the spectral shape is mostly due to collective modes and the three lines structure for
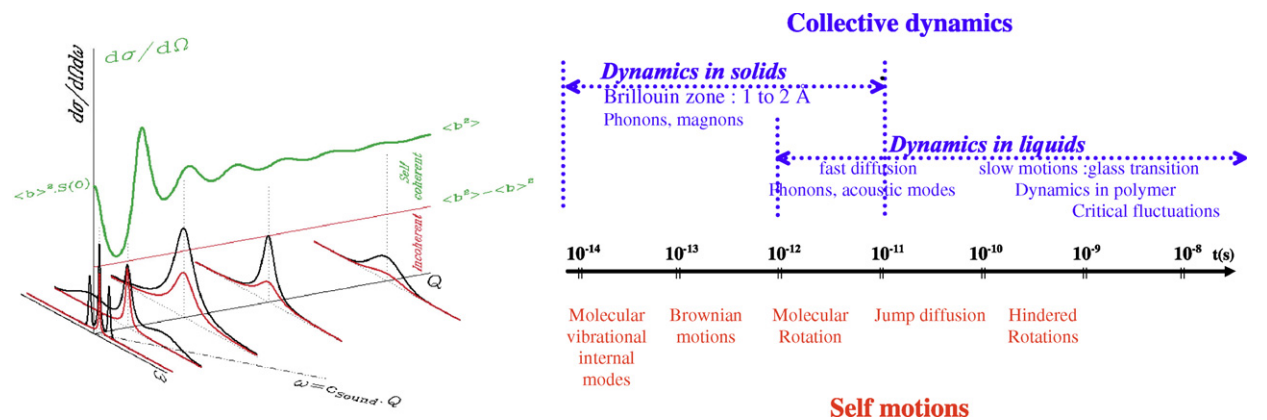

Fig. 1. Left: This figure highlights the different contributions to the neutron intensity scattered by a liquid sample. The full black and red curves picture, at selected Q values, the two terms into brackets of Eq. (3): respectively the coherent and incoherent inelastic contributions (for the sake of clarity, the only purely inelastic excitations figured here are the low frequency coherent ones—see text). After integration over energy, the latter reduces to a flat background (thin red line) over which oscillates the structure factor $S(Q)$ (green curve). Both terms are formalized in Eq. (4). It is actually this quantity $d\sigma/d\Omega$ which is typically measured on a liquid diffractometer wherein the neutrons are counted regardless to their scattered energy. It should be noted that this quantity differs from $S(Q, \omega = 0)$. Right: Summary of the various dynamics (collective excitations in the upper part and self motions in the lower part) as a function of their characteristic relaxation times.

$S(Q \approx 0, \omega)$ corresponds to the Rayleigh line (entropy fluctuations) and the Brillouin doublet (pressure fluctuations) well known in light scattering experiments. The propagating modes at $\omega = c_s Q$ (with c_s the velocity of sound) are well defined for liquid metals for $Q < 1$ Å^{-1}. The width of these collective excitations increases with Q, leading to an overlap of the 3 peaks.

For Q equal or larger than the position of the first structure peak, $S(Q, \omega)$ shows, as a function of ω, a relatively sharp peak centred on $\omega = 0$ (non-propagating mode); its width $\Delta\omega$ is a characteristic of (i) either the lifetime for a group of atoms to act together (whole molecule translational vibrations and librations); or (ii) of the characteristic time for a diffusive step of a given atom (self motions: diffusion, reorientation; as seen in Section 6.3 the analysis of the Q dependence allows separating between rotational and translational motions). Then the quasielastic widths $\Delta\omega$ ($\omega \approx 0$) for coherent and incoherent scattering are similar (characteristic times from 10^{-12} to 10^{-10} s).

Besides this quasielastic contribution, the modes of internal molecular vibration show up as inelastic peaks located at higher energy transfers (gain and loss of neutron energy; characteristic times from 10^{-14} to 10^{-13} s).

At large Q limit, the collective modes are completely damped, and the observed spectrum is given by the self term of the space time correlation function. In the perfect gas limit the inelastic line is a Gaussian distribution around $\omega = 0$ with a width $\Delta\omega = \sqrt{k_B T / M}$, M being the mass of the scatterer (no interaction between scattering centres probed in this Q range).

The energy integration of $S(\mathbf{Q}, \omega)$ defines the '*total*' structure factor $S(\mathbf{Q})$. From Eq. (2), $S_{\text{tot}}(\mathbf{Q})$ is then the Fourier transform of the instantaneous space correlation function $G(\mathbf{r}, 0)$

$$S_{\text{tot}}(\mathbf{Q}) = \int_{-\infty}^{\infty} S(\mathbf{Q}, \omega)\,d\omega = \int_{-\infty}^{\infty} \delta(t)\,dt \int_V \exp[i\mathbf{Q}.\mathbf{r}]\big[G(\mathbf{r}, t) - \rho\big]\,d\mathbf{r} = \int_V \exp[i\mathbf{Q}.\mathbf{r}]\big[G(\mathbf{r}, 0) - \rho\big]\,d\mathbf{r}$$

and gives a 'snapshot' of the structure of the system. Conversely the '*elastic*' structure factor corresponds to infinite time exposure,

$$S_{\text{el}}(\mathbf{Q}, \omega = 0) = \int_V \exp[i\mathbf{Q}.\mathbf{r}]\big[G(\mathbf{r}, \infty) - \rho\big]\,d\mathbf{r}$$

In two axis neutron structure experiments the measured intensity $I(2\theta)$ gives the number of neutrons scattered with the angle 2θ within the solid angle $d\Omega$, regardless of their energy exchanges with the sample. In a crystal diffraction experiment, atoms only vibrate about their equilibrium position and the snapshot is a good approximation of the time averaged structure: Bragg scattering is almost purely elastic ($k_0 = k$) and thermal vibrations are responsible for a Debye Waller factor. In the case of liquids (or gas), the scattering involves dynamic processes. The experimental signal is equivalent to an integration of the double differential scattering cross-section over all possible energy transfers (limited to the incident energy $\hbar\omega_0$ of the neutron)

$$I(2\theta) = \left.\frac{d\sigma}{d\Omega}\right|_{2\theta} = \int_{-\infty}^{+\hbar\omega_0} \left.\frac{d^2\sigma}{d\Omega\,d\omega}\right|_{2\theta} d\omega$$

The static approximation is valid if the energy transfers with the liquid are small compared to the incident neutron energy (i.e. $\tau_{\text{snapshot}} \ll \tau_{\text{liquid}}$ where $\tau_{\text{snapshot}} \sim 2\pi/\omega_0$). This condition is always fulfilled with X-ray scattering for which $\tau_{\text{snapshot}} \approx 10^{-18}$ s. For neutron scattering, $\tau_{\text{snapshot}} (\propto 1/\lambda^2)$ varies from a few 10^{-12} s for cold neutrons to a few 10^{-15} s for hot neutrons and the static approximation is more questionable and leads to inelasticity corrections to obtain $I(Q)$ from the measured $I(2\theta)$ (see [2] for an extensive discussion).

For a homogeneous isotropic system (i.e. applying the spherical symmetry) and within the static approximation, the scattered intensity $I(Q)$ is the sum of a structured coherent term and a flat (Q-independent) incoherent component,

$$I(Q) = \int_{-\infty}^{\infty} \left.\frac{d^2\sigma}{d\Omega\,d\omega}\right|_{Q\,\text{cst}} d\omega = \langle b^2 \rangle \int_{-\infty}^{+\hbar\omega_0} \frac{k}{k_0} S(\mathbf{Q}, \omega)\,d\omega = \langle b \rangle^2 S(Q) + \big(\langle b^2 \rangle - \langle b \rangle^2\big) \tag{4}$$
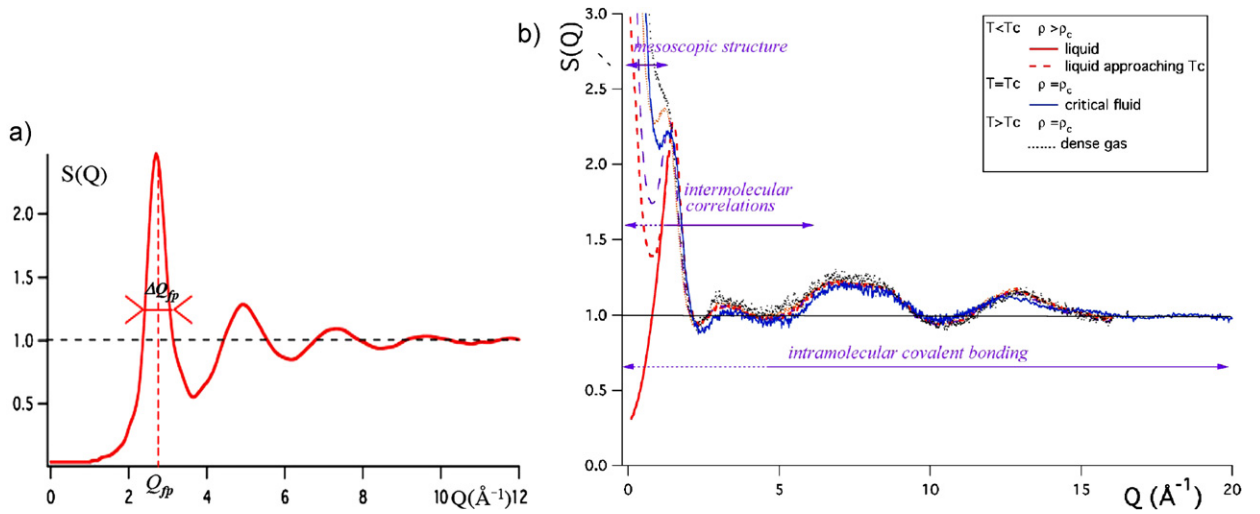
Fig. 2. (a) Structure factor of liquid aluminium. (b) $S(Q)$ for a molecular liquid (C_2D_6) (thick full line). When approaching the critical temperature T_c, the raise at low Q is characteristic of the density fluctuations accompanying the gas–liquid transition. Broken lines are for thermodynamic points approaching the critical point from the liquid side ($\rho < \rho_c$, $T > T_c$). The thin full line is for the critical fluid ($\rho = \rho_c$, $T = T_c$). For $T > T_c$ on the critical isochore, $S(Q)$ is typical of that of a dense gas (dotted lines). Measurements with $\lambda = 0.7$ Å have been completed by an experiment with $\lambda = 0.5$ Å in order to reach the completion of oscillations at large Q, necessary for an accurate adjustment of the intramolecular contribution.

The pair correlation function $g(r)$ giving the correlation between distinct particles is defined by

$$G(r, 0) = G_s(r, 0) + G_d(r, 0) = \delta(r) + \rho g(r)$$

$$S(Q) = 1 + \frac{4\pi\rho}{Q} \int_0^{+\infty} r\big(g(r) - 1\big) \sin(Qr)\, dr \quad \text{or} \quad r\big(g(r) - 1\big) = \frac{1}{2\pi^2\rho} \int_0^{+\infty} Q\big(S(Q) - 1\big) \sin(Qr)\, dQ \qquad (5)$$

Fig. 2(a) shows a typical structure factor of a simple monoatomic liquid. Empirically, the first peak with a maximum at Q_{fp} and a width ΔQ_{fp} gives the average distance $r_{fp} = 7.4/Q_{fp}$ (simple liquid evaluation) and the spatial extent of the short range order $L_{SRO} = 2\pi/\Delta Q_{fp}$. Fig. 2(b) illustrates the behaviour of a molecular liquid at the approach of the liquid–gas phase transition. From a theoretical point of view, the precise knowledge of $S(Q)$ for Q going from 0 to infinity allows a complete description of the instantaneous microscopic and mesoscopic structure of the liquid. From an experimental point of view, one has to choose between various instruments with different accessible Q ranges (cold, thermal or hot neutrons from reactors or Time-of-Flight (TOF) neutrons on pulsed source) to focus respectively on mesoscopic structure ($Q < 0.3$ Å^{-1}), heterogeneity or aggregates ($0.02 < Q < 0.5$ Å^{-1}), local order due to nearest neighbours ($0.1 < Q < 12$ Å^{-1}) with information on intermolecular ordering in the lower part of this range, covalent intramolecular bonding ($5 < Q < 50$ Å^{-1}). In order to obtain a good accuracy on the pair correlation function, the Q domain has to extend up to the completion of the oscillations of $S(Q)$, i.e. up to about $Q_{max} = 25$ Å^{-1} or beyond (see Fig. 2(b)). This corresponds to $\lambda = 0.5$ Å, which is the domain of neutrons produced by a hot source (or X-rays of about 20 keV). Hot sources on major facilities (ILL, LLB, FRM-II), and the spallation sources (ISIS, SINQ, IPNS) provide short neutron wavelengths. Some diffractometers (D4c [ILL], 7C2 [LLB]) are optimized for the study of the structure of liquid or amorphous matter (low resolution, high intensity).

The case of polyatomic liquids is more complex as the scattered intensity depends not only on the concentration of the different atomics species, but also on their relative scattering lengths b_i. For a diatomic liquid AB a full (statistical) description including the chemical order of the average structure involves the partial pair correlation functions $g_{AA}(r)$, $g_{AB}(r)$, $g_{BB}(r)$, which are related to the partial scattered intensities $S_{AA}(Q)$, $S_{AB}(Q)$, $S_{BB}(Q)$, through a relation analogous to (5) (for more detail see Appendix 4 in [1]). Experimentally, the total $S(Q)$ is measured and related to the partial intensities by:

$$S(Q) - 1 = \big(c_A^2 b_A^2\big[S_{AA}(Q) - 1\big] + 2c_A b_A c_B b_B\big[S_{AB}(Q) - 1\big] + c_B^2 b_B^2\big[S_{BB}(Q) - 1\big]\big)/(c_A b_A + c_B b_B)^2 \qquad (6)$$

where c_i is the concentration of atoms i and b_i the corresponding scattering length.

As a consequence, the Fourier transform of $S(Q)$ gives a pseudo pair correlation function $g(r)$ which is scattering length dependent. One method to obtain the partial structure factors is to use neutron diffraction isotopic substitution (NDIS), but this is a difficult and expensive technique as several samples have to be used with various isotopic contents [2,3]. In some systems (multicomponent or molecular), the analysis of the structure of the liquid can be done by modeling $S(Q)$ in such a way that the various correlations are separated according to the strength of the interaction (pairs of atoms involved in intramolecular covalent bonding, correlations between molecules, aggregates or density fluctuations). Some examples of applications of this method will be given in the following.

2.2. Other spectroscopies (X-ray scattering and absorption)

X-ray diffraction was used in the 1930s for the study of liquids, and then rapidly left aside with the advent of neutron beams due to the intrinsic properties of neutrons: large penetration depth allowing complex sample environments, absence of atomic form factor, ... With the advent of third generation synchrotrons, the situation evolved as the brilliance of X-ray sources is so high that the damping by absorption is overcome. A focussing size down to 10 μm is now a standard and the possibility to reach extreme conditions of pressures (megabar range with the diamond anvil cells) and temperatures (2000 K and beyond by laser heating) opened new doors for the benefit of e.g. the earth sciences. In addition, a large spectrum of wavelengths is span by the X-rays, say from 0.1 to 1 Å, values well adapted for the study of liquids.

An alternative to neutron diffraction using isotopic substitution to access the partial structure factors is the anomalous X-ray diffraction (AXD) taking advantage of the energy dependence of scattering lengths. Practically, in order to have a good signal-to-noise ratio, for non-absorbing isotopes, the quantity of material amounts to several cubic centimetres at least for neutron scattering and 10^{-1} mm^3 for synchrotron X-rays.

In addition, the tunability of X-rays allowed the development of X-ray absorption: XANES (X-ray absorption near edge structure) and EXAFS (Extended X-ray absorption fine structure) are local probes that measure the local environment of an atom of a given species by an energy scan around an ionisation threshold. In Section 3.2.1, we show that combined neutron and EXAFS experiments give access to the SRO and the chemical order. The experimental determination of the higher order correlation functions is out of reach of experimental techniques. Fortunately, as seen in the next section, the computer simulations help.

The measurements of physical parameters—such as densities (required for the neutron and X-ray data reduction), conductivities, susceptibilities, etc.—are of great value even if they are not directly related to the structure.

2.3. Computer simulations

The theoretical tools are of two types (analytical and numerical):

(i) Analytic theories (in addition to the calculation of interactions: integral equations, renormalisation theory, ...). They played an important role in the 1960s or 1970s but were superseded by the computer simulations [4].
(ii) Computer simulations. There are various kinds of approach.

Two ingredients are necessary to model a liquid at thermal equilibrium: the interaction energy and the entropy coming from the disorder. The former is the easiest part: numerous interaction potentials or total energies are available, at different levels from the oversimplified hard core potential to the most sophisticated ab initio total energy calculations. The entropy is far more difficult to model as it is a collective effect by nature. The translational degrees of freedom are continuous variables and the entropy is uneasy to compute as a difference with the substitutional alloys for which the disorder is discrete and the correlation functions as well.

Historically, the advent of the fast computers played an important role in our understanding of the liquid state, early in the 1960s. Indeed, the entropy is automatically generated in the computer simulation. Limitations in time and spatial extension of the computer simulation experiments are of the order of several picoseconds and nanometers. If the computer simulations are highly valuable to describe local order, they are more limited to describe the vicinity of critical points where some quantities diverge and go beyond the size of the simulation box.

Various kinds of approach can be cited (see [5,2] and references therein for an extensive discussion):

(a) Monte Carlo (MC) techniques (random displacements of atoms with respect to a given interatomic potential) used to compute average quantities at thermodynamic equilibrium under the assumption of ergodicity. Depending on the level of description of the interactions, the technique involves between hundreds to tens of thousands of atoms.

(b) Molecular dynamics (MD) allow the calculation of the trajectories of individual particles by solving numerically the Newton's equations of motion for the atoms; then a time average calculation of the properties is made. Both equilibrium and non-equilibrium quantities are accessible. MD ab initio methods aimed at overcoming the calculation of a pair potential since they are based upon a quantum mechanical treatment of the valence electrons. Depending on the level of description of the interactions, the technique involves between 50 to thousands of atoms and sampling times of the order of the picosecond.

(c) Reverse Monte Carlo (RMC) [5] simulation for which the 'driving force' is the agreement between the calculated structural model (three-dimensional configuration of *n* atoms, without any interaction potential assumption) with experimental measurements, taking into account the data uncertainties. Data sets from different measurements (set of NDIS data for the partial structure factors refinement) or different experimental techniques (neutron and X-ray scattering, EXAFS, NMR, electron diffraction, …) can be fitted simultaneously; an example is given in Section 3.2. An alternative method coupling RMC with interatomic potential refinement is the Empirical Potential Structure Refinement (EPSR) largely used for the simulation of liquid structure. The key point to be discussed using both RMC and EPSR calculations is that the configuration obtained is consistent with the data, but not the unique one; the influence of the input constraints has also to be cautiously considered. Besides, these tools are efficient to establish a structural model and helpful to a comprehensive approach of the liquid configuration.

3. Liquid metals and covalent liquid alloys

3.1. Simple liquid metals: SRO in undercooled liquid Nickel

Many books and review papers have been written on the structure and the dynamics of liquid metals [6–9]. Since the pioneering work of Turnbull, it is now well known that a great variety of pure metals can be undercooled below their melting temperature [10]. Studies on deeply undercooled metals have recently taken advantage of technical improvements such as electromagnetic levitation facilities.

In this section, we present recent results concerning the study of short range order in undercooled liquid Nickel. F.C. Franck suggested that an icosahedral short range order (ISRO) could explain the observed undercooling [11]. This hypothesis relies on the fact that, for a standard interaction potential, the energy of a 13 atoms icosahedral isolated cluster is lower (i.e. more stable) than the energy of a 13 atoms fcc or hcp cluster, due to a surface tension effect. Later on, molecular dynamics calculation confirmed this idea [12,13] but no direct experimental proof was given.

Using grazing incidence X-ray diffraction, Reichert et al. [14] showed a five-fold local symmetry of the liquid Pb deposited on a Si(001) surface. However, a direct investigation of the bulk melt, essential to understand the mechanism of nucleation of the solid phase in the liquid one, was still lacking.

A containerless setup using a levitation technique [15,16] was made by the group of Holland–Moritz in order to study the local order in deeply undercooled metallic melts [17]. Fig. 3(a) represents the structure factor for liquid Ni at various temperatures above and below the melting point ($T_m = 1728$ K). It is characteristic of metallic systems with a first well-defined peak and, in addition, a shoulder on the right-hand side of the second oscillation. This shoulder is not observed in the structure factors of monoatomic metallic liquids and should be therefore characteristic of a particular SRO. In order to check the hypothesis of ISRO, a simulation of the structure factor for large Q values (see Section 4.1) was performed (Fig. 3(b)). In the case of undercooled liquid Nickel, the modelling allowed discriminating between different geometries of clusters present in the liquid (bcc, fcc, hcp, icosahedral, and dodecahedral) and some authors concluded on the existence of an ISRO [17]. The issue is still a subject of discussion.

3.2. Covalent liquids

In 1960 Joffe and Regel [18] proposed to distinguish between liquid metals and liquid semiconductors using the electrical conductivity σ as the relevant parameter. A liquid is metallic if $\sigma > 2000\ \Omega^{-1}\ cm^{-1}$ and semiconducting if $\sigma < 300\ \Omega^{-1}\ cm^{-1}$. An increase of σ with temperature can also be used as a criterion to identify a liquid semiconductor. Apart from the electrical conductivity, covalent liquid semiconductors very often show structural properties
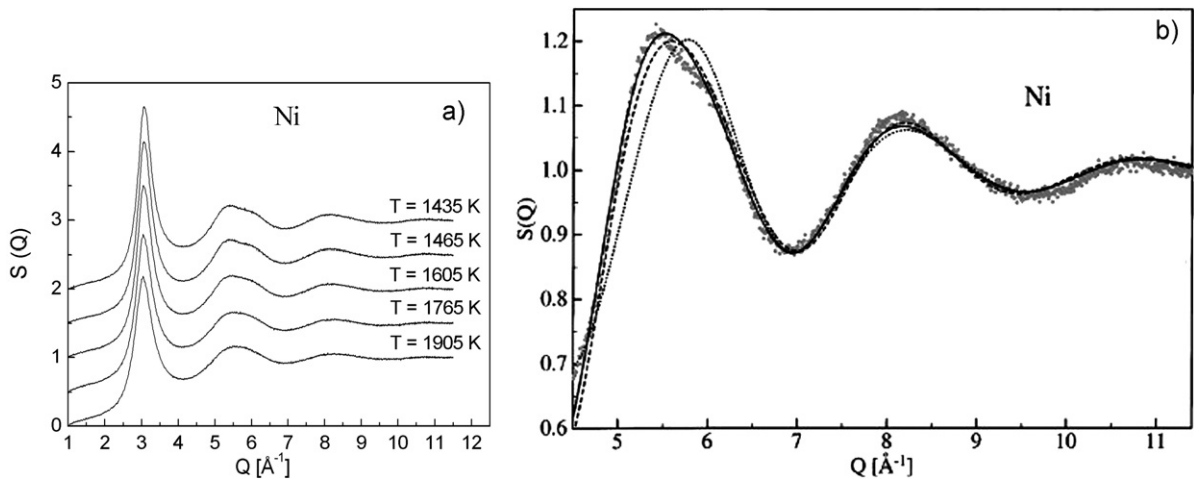
Fig. 3. (a) Experimental structure factor of undercooled liquid Ni at various temperatures above and below $T_m = 1728$ K. The curves are shifted in order to ensure legibility. (b) Comparison between the measured $S(Q)$ at $T = 1435$ K (dots) and simulated structure factors when assuming clusters with different symmetries prevailing in the melt: icosahedra (dashed line), dodecahedra (solid line) and fcc clusters (dotted line). Reproduced from [17].

which are different from most metallic liquids. Theoretical studies indicate that the origin of these structural features can be found in the presence of directed covalent bonds in the liquid.

Two recent studies concerning the structure of multi-component covalent liquids are presented. We consider, first, binary liquid of germanium–telluride which shows a density anomaly around its eutectic composition $Ge_{0.15}Te_{0.85}$. This example proves the necessary complementarity between neutron scattering and X-ray absorption spectroscopy techniques. Then we focus on ternary Te-based chalcogen alloys, that are potential candidates as materials for RAM memories and optical data storage. We show how a study of the short range order of liquid alloys could allow selecting the good candidates for technical applications. The structure of covalent materials is driven by the Peierls distortion (quantum mechanical spontaneous symmetry breaking mechanism). It has been shown that the Peierls distortion may exist in the absence of translational symmetry [19] and that it plays some role to create a negative thermal expansion.

3.2.1. Negative thermal expansion in GeTe alloys

Liquid alloys of germanium and tellurium exhibit a series of thermodynamic anomalies in a temperature range between the eutectic temperature (650 K) and 750 K and in a composition range between pure Te and about 20% Ge. The most intriguing one is the density anomaly: the molar volume is passing through a minimum in the liquid state [20]. This behaviour is linked to a maximum in specific heat and an increase of the electrical conductivity by two orders of magnitude in a 200 K range at the eutectic $Ge_{0.15}Te_{0.85}$ composition [21]. Despite great experimental effort, up to now the underlying mechanisms are not yet understood in detail.

Neutron scattering experiments have the potential to contribute the understanding of the structure of these liquid alloys. However for multi-component systems, the very expensive isotopic substitution is needed to obtain the partial pair correlation functions. To overcome this difficulty, one combines different experimental techniques and computer simulations. One of the most used simulation technique in liquids is the so-called Reverse-Monte Carlo Method (RMC) first introduced by McGreevy et al. to study disordered materials by calculating the atomic structure consistent with neutron scattering experiments [22]. Recently a RMC study was published which uses at the same time neutron scattering and X-ray absorption measurements to understand the local order of liquid GeTe in detail [23].

The basic idea is to include the chemical selectivity of the X-ray absorption spectroscopy in the RMC calculation and keep at the same time the high accuracy information of the neutron experiments. While the total structure factor obtained by neutron scattering [24] is not sufficient to get a detailed view of the local structure, it is well demonstrated that the XAS data alone with RMC give questionable local geometries due to the over-simplified assumptions to describe the disorder in the liquid. By bringing together the neutron and X-ray data and the RMC method (Fig. 4), it was possible to describe consistently the density anomaly as a structural change from a liquid with a Peierls like symmetry
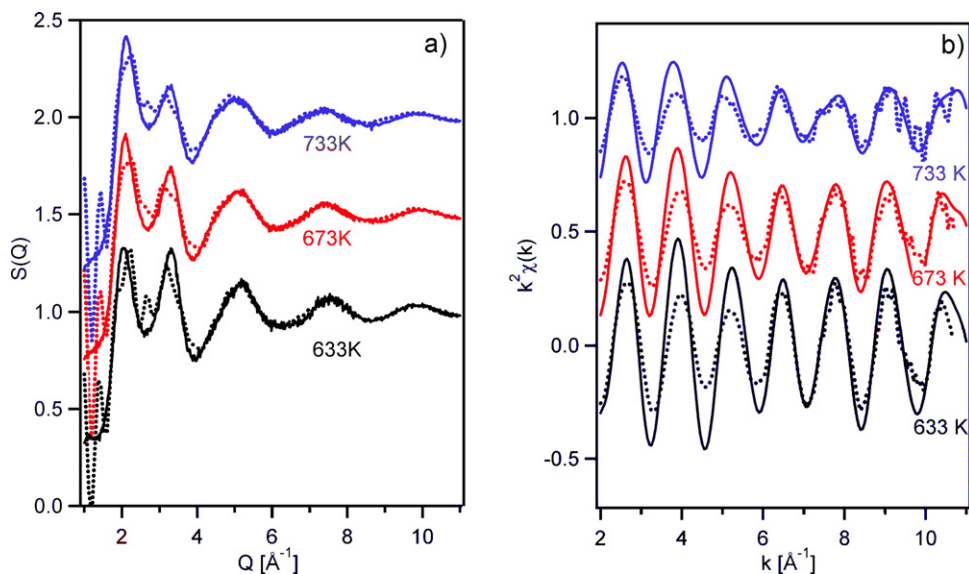
Fig. 4. Neutron scattering and EXAFS measurements of $Ge_{0.15}Te_{0.85}$ liquid alloys at various temperatures. (a) Experimental total structure factor (full lines) and the corresponding result of the RMC fit (dashed lines). (b) Experimental EXAFS function $k^2\chi(k)$ measured at Ge K-edge (full lines) and the corresponding result of the RMC fit (dashed lines). The curves are shifted to ensure legibility. The figures are reproduced from [23] and [24].

broken local environment at low temperatures to a more symmetric local environment at higher temperatures which is stabilized by gain of entropy [23,25].

3.2.2. Phase change materials

With the increasing development of data storage and memory devices using the optical and electrical properties of phase-change (PC) materials, the tellurium-based ternary alloys have been the subject of an intense activity [26]. Among them, the reference materials for commercial DVD-RAM are the pseudo-binary chalcogenide compounds $(GeTe)_2$–Sb_2Te_3 (or $Ge_2Sb_2Te_5$) as they have good optical and electrical contrast. More precisely, the GeSbTe phases have the ability to crystallise easily and amorphise under the action of a laser pulse, a basic process of commercial phase-change optical disks. During this reversible process, the crystal is locally melted to obtain an amorphous spot (crystal–liquid–amorphous transitions): this corresponds to the recording process. In a second time, this spot can be recrystallised (amorphous-crystal transition) by using a less intense laser beam; this is the erasing process.

Recently, microscopic models of the amorphous and crystalline states have been suggested to explain the working mechanisms of PC-materials [27,28]. However, much less was known about the liquid state of these materials despite its prominent role for both amorphisation and recrystallization. Indeed, amorphisation is achieved by quenching the liquid, while the fast recrystallization of amorphous regions takes place above the glass-transition temperature, suggesting that it might proceed through the under-cooled liquid state.

Therefore an in-depth knowledge of the structure of the liquid state could improve the understanding of both the amorphisation and the recrystallization mechanisms. Many ternary Te-based alloys were studied in the liquid state by neutron scattering [29]. Fig. 5 represents the structure factors obtained for various alloys. In ternary alloys, the total structure factor is the summation of six partial structure factors and, as recalled in Section 2, without complementary experiments, it is impossible to perform a quantitative analysis of the short range order in such liquid systems. However, in these systems a qualitative analysis is possible as the structure factors presented in Fig. 5 are showing strong variations of the first two peaks. The ratio between the heights of these first peaks is then used as fingerprint for a given local arrangement. In such a way, two classes of liquids were defined. For the first class with a low number of electrons per atom ($N_{e/a} < 4.5$), the structure of the liquid is tetrahedral-like similarly to the solid and the contrast in electrical/optical properties is not sufficient to qualify the material for PC availability. On the contrary, the second class of materials with a higher number of electrons per atom ($N_{e/a} > 4.5$) has an octahedral-like local structure and possesses a PC capability. In parallel to the experimental analyses, computer simulations of the liquid structure are
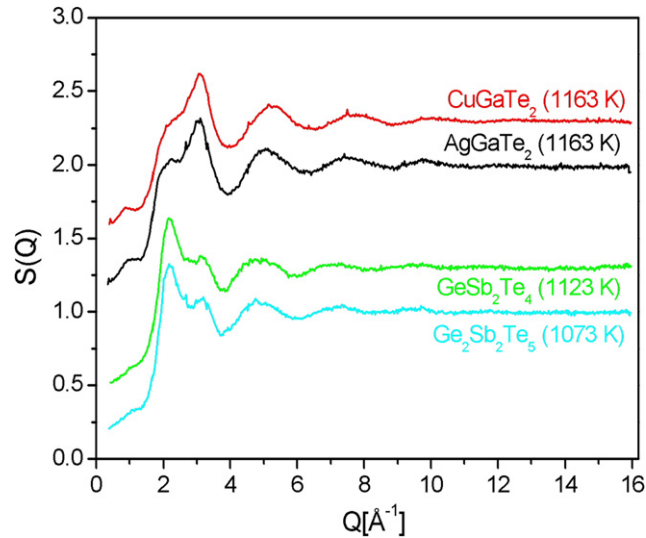
Fig. 5. Experimental total structure factor $S(Q)$ of several Te-based ternary alloys with $N_{e/a} < 4.5$ (tetrahedral liquids, upper part) and $N_{e/a} > 4.5$ (octahedral liquids, lower part). The curves are shifted in order to ensure legibility.

performed, in good agreement with the experiments. From the ab initio MD experiments, a detailed analysis of the local order can be made.

In conclusion, a systematic study of the liquid structure of covalent alloys gives access to relevant parameters in relation to the PC capability, and contributes to the fundamental understanding of the driving forces for the transition between tetrahedral and octahedral environments.

4. Molecular liquids: intramolecular structure and dynamic disorder

For many molecular liquids the rotational motions of the molecules do not freeze at the same temperature as the translational motions. In the case of globular highly symmetric molecules (i.e. experiencing isotropic reorientation), the freezing of translational motions appears first: the centres of mass of the molecules occupy the sites of a regular crystal lattice, giving rise to Bragg intensity, but the molecular orientations remain largely disordered and the Bragg peaks are strongly damped with increasing Q. Nevertheless, it has been shown [30] that the analysis of the diffuse background obtained by neutron scattering at large momentum transfers allows to determine with accuracy the intermolecular structure. This method has been applied successfully to obtain a precise determination of the geometry of rigid rotating molecular entities such as ND_3 [31], $Me(ND_3)_n$ [32,33] or C_{60} [34,35]. This methodology can be extended to the case of molecular liquids. Assuming that the fluctuation of one atom around its equilibrium position can be divided into a translational motion of the molecular centre of mass and an intramolecular rotation and vibration and neglecting the orientational correlation between molecules [30], the total scattering intensity can be written by analogy to Eq. (4) as

$$\frac{d\sigma}{d\Omega} = \langle F \rangle^2 S_{cm}(Q) + \left(\langle F^2 \rangle - \langle F \rangle^2 \right) \tag{7}$$

where $\langle F \rangle$ is obtained as the statistical average of the molecular form factor F: $\langle F \rangle = \sum_{i\,(molecule)} \langle b_i \exp(iQ \cdot r_i) \rangle$ with r_i referring to the position of the atom i within the molecule; $S_{cm}(Q)$ is the structure factor of the molecular centres of mass and can be expressed as the Fourier transform of the centre of mass pair correlation function $g_{cm}(r)$:

$$S_{cm}(Q) = 1 + \rho_m \int \exp(iQ \cdot r) \{ g_{cm}(r) - 1 \} \, dr \tag{8}$$

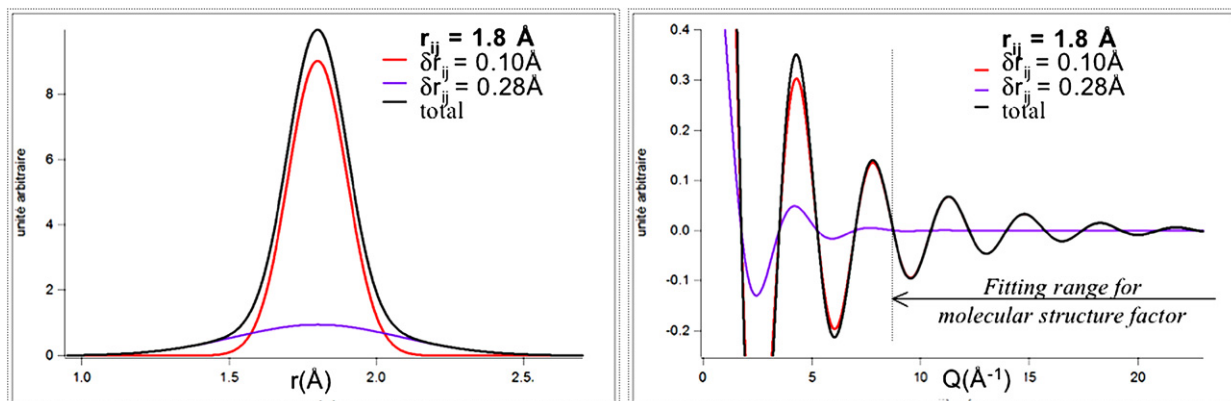in which ρ_m is the molecular number density.

Fig. 6. Separation in Q-space of two contributions to the total $S(Q)$ overlapping in r-space with different strengths. Left: The total contribution to $g(r)$ is given by the black line in r-space. The red line is for a well defined order correlation length as that resulting from covalent bonding (small mean quadratic fluctuation $\langle\delta r^2\rangle$) while the cyan one is characteristic of a smoother intermolecular interaction (with a larger mean fluctuation). On the right, these contributions to the total $S(Q)$ are represented in Q-space using the same colour code. It can be seen that the smoother correlation is rapidly damped by its factor $\exp(-\langle\delta r^2\rangle * Q^2/2)$ and that the more tight order alone propagates at large Q value.

The intramolecular contribution is given by

$$\langle F^2\rangle = \sum_i \sum_j \left[b_i b_j j_o(Qr_{ij}) \exp\left(-\frac{1}{2}\langle\delta r_{ij}^2\rangle Q^2\right)\right] \tag{9}$$

where the b are the atomic scattering lengths, r_{ij} is the distance between atoms i and j in the same molecule, δr_{ij} is the mean deviation of r_{ij} and j_0 is the spherical Bessel function of the first kind and of order 0.

At large Q values the leading term in Eq. (7) is the molecular structure factor $\langle F^2\rangle$ since the intermolecular contribution $\langle F\rangle^2 (S_{cm}(Q) - 1)$ is strongly damped due to the wider distribution of the distances between the molecular centres of mass, as compared to best defined intramolecular distances (see Fig. 6). It is then possible to determine with accuracy the molecular structure from a direct fit of $S(Q)$ in a Q range where the intermolecular term is vanishing.

Fig. 6 illustrates the separation of two different interactions with the same distance of 1.8 Å. The intramolecular contribution is accounted for by covalent bonding, resulting in a well defined bond length ($\delta r = 0.10$ Å); this gives an oscillating Q function propagating at high Q value. As a difference the softer intermolecular correlation (with fluctuation $\delta r = 0.28$ Å) is strongly damped and no longer detectable in $S(Q)$ for Q larger than 8 Å^{-1}.

The relevant criteria allowing an accurate adjustment of the intramolecular term are the limits of the fitted Q-range, the number of independent parameters, and the description of molecular dynamic disorder. The stability of the fitting procedure, the analysis of the covariance matrix and the quality factor when determining the Q-range are crucial tests for a correct evaluation of the short range rigid interactions. For a molecular entity containing n atoms, $n(n-1)/2$ intramolecular distances and their quadratic fluctuations are involved in Eq. (9). The intramolecular distances are given as a function of the covalent bond lengths and the inter-bond angles. Their average fluctuations are calculated using a composition of the quadratic deviations of these independent parameters [35,42]. In the case of liquids with small rigid groups (for example $-CD_3$ or $-ND_3$ groups), the number of fitted parameters can be reduced, taking into account their internal rotation (or libration) [31].

The last step consists in subtracting the intramolecular contribution to the total structure factor. The residual signal obtained in the low Q-range is characteristic of the less rigid intermolecular correlations.

This approach has been used to determine the SRO in various systems, either using simulation of the experimental signal at large Q (for example liquid Ni [17], liquid sulfur [36], liquids forming quasicrystals [37] or the S–Te liquids [38]) or performing a least square adjustment of the structure factor in the pertinent Q range (for example in H-bonded liquids such as H_2O [39], NH_3 [40], or solvents displaying a peptidic group as N-Methyl Formamid (NMF) [41,42] and N-Methyl Acetamid (NMA) [40]). Some examples are given below.

4.1. Structure of liquid sulfur near the lambda transition

This methodology has been applied to the study of the polymerization transition of liquid sulfur occurring at $T = 432$ K at the microscopic level [36]. Below the transition temperature, the liquid is shown to mainly consist of S_8 molecular units; with increasing the temperature the rings are progressively breaking into long chains. The analysis of the structure factor measured at large angles allows one to follow the change in the local order giving access to slightly different contributions from the various S–S pairs: intra-ring, intra-chain and inter-chain. Above the transition temperature, the presence of large polymerized units is shown by small angle neutron scattering [43].

4.2. Characterization of the rotational dynamic disorder in liquid ethane (C_2D_6)

The structure factor of deuterated ethane has been obtained by means of large angle neutron scattering on the liquid diffractometer D4c (ILL) for $\lambda = 0.7$ ($E_{inc} \approx 160$ meV) and 0.5 Å ($E_{inc} \approx 320$ meV) and the outline of this experiment is given in Fig. 2(b). It has been shown [42,45] that the quality of the adjustment of the intramolecular contribution using Eq. (9) in the [3.8–13.8 Å^{-1}] Q range is improved when taking into account the torsional motion of the rigid –CD_3 groups responsible for a distribution in some intramolecular distances ($C_i - D_j$ and $D_i - D_j$). This dynamic disorder can be realistically described by the density function $P_n(\varphi)$ for the deuterium localisation on the circles defined by the internal rotation [31] with $\delta\varphi$ the mean amplitude of libration.

$$P_n(\varphi) = n \frac{1}{2\pi I_0(\gamma)} e^{\gamma \cos(n\varphi)}, \qquad \delta\varphi = \frac{1}{n} \cos^{-1}\left(\frac{1}{\tanh(\gamma)} - \frac{1}{\gamma}\right) \tag{10}$$

with n the number of sites (3 for a methyl group), γ the libration parameter (which goes from 0 for free rotation to infinity for localised sites) and $I_0(\gamma)$ the modified Bessel function of the first kind and order 0.

The adjustment of the molecular term implies 7 structural parameters: two bond lengths r_{CC}, r_{CD}, the C–C–D_3 angle α, their fluctuations and the libration parameter γ. The fit returns $\gamma = 1.79$ corresponding to a half width at half height of $\theta = 20.03°$ which is in good agreement with spectroscopy results (for C_2D_6, the energy of the ground state of libration is calculated 9 meV ($\tau \approx 10^{-13}$ s) with a hindering barrier to rotation of about 125 meV [44]). In a previous work [45], 10 parameters were used to define the molecular geometry without introducing the rotational disorder and an unrealistic result ($\delta r_{D_i D_j}(\pi/3) < \delta r_{CC}$, as defined in the insert of Fig. 7) was obtained.
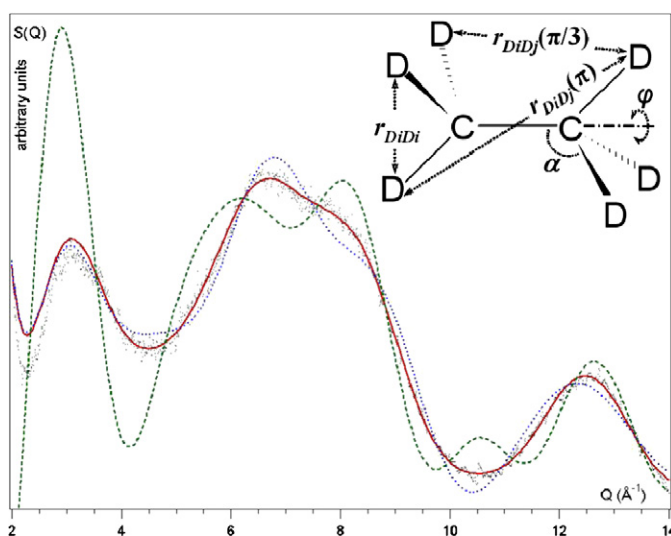

Fig. 7. Structure factor of liquid C_2D_6: Experimental curve, best fit obtained for $\gamma = 1.79$ (bold line) and simulations for $\gamma = 0$ (free rotation: dotted line) and $\gamma = 100$ (no libration: dashed line). The molecular geometrical parameters are given in the insert. Reproduced from [42].
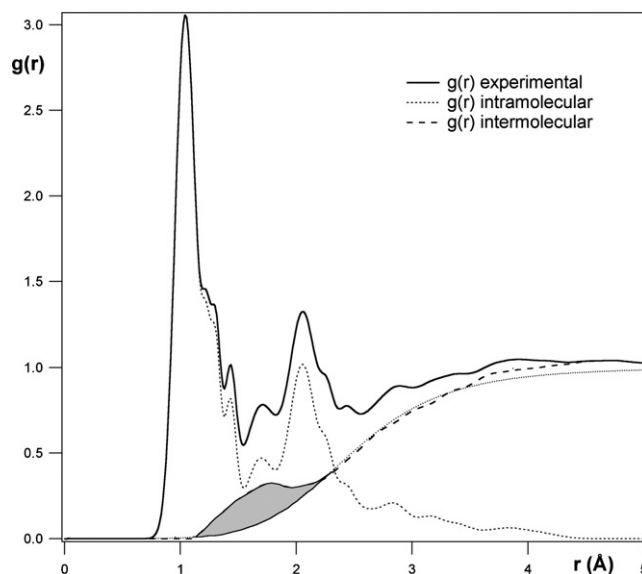
Fig. 8. Fully deuterated NMF pair distribution function. The experimental $g(r)$ (thick line) is split into intramolecular (dotted line) and intermolecular (dashed line) terms. The first bump in the latter (grey shaded) is accounted for by H-bonding at 1.72 Å [42].

4.3. H-bonding in molecular liquids

The adjustment of the molecular structure of N-methylformamide has been carried out for trans or cis conformations, assuming 3 deuterium sites or free rotation for the methyl groups [40,42].

The best result is obtained for $7 < Q < 23$ Å^{-1} for a trans conformation with a free rotation of the methyl. Fig. 8 reports the pair distribution function $g(r)$ and the inter and intra contributions. The hydrogen bond shows up in the intermolecular term with a characteristic length of 1.72 Å and a mean fluctuation of about 0.31 Å. The fit indicates that approximately 56% of the molecules are hydrogen bonded. As a difference with a previous study using the H/D isotopic effect [41], it has been possible to characterize H bonding from a direct fit of the structure factor of the fully deuterated compound.

5. Structure and dynamics in supercritical fluids

For the last thirty years, there has been a continuous increase of the use of supercritical fluids (SCF) (mainly H_2O and CO_2) for industrial applications. While carbon dioxide allows extraction of undesirable substances (such as caffeine, one of the first applications of CO_2) at temperatures close to ambient condition, supercritical water can eliminate organic wastes by oxidation. Physical and chemical properties are strongly modified in the supercritical state, such as the molecular mobility which is strongly enhanced. Consequently, chemical reactions the kinetics of which is controlled by diffusion can be monitored by changing the density of the SCF, which can be tuned from gas to liquid densities. In this context, numerous fundamental studies have been devoted to the microscopic structure and dynamics of SCF. For instance, the persistence of some hydrogen bonding in supercritical water, determined from neutron diffraction experiments, was a subject of debate [46,47]. The dynamics was also investigated by quasi-elastic and inelastic neutron scattering [48,49]. Among other results, it was shown that the residence time τ_0, which slightly increases upon decreasing the density, is 10 times shorter than that in ambient liquid water. From a more academic point of view, there is a strong interest for SCF close to their critical point where scaling and universality behaviour can be observed. An example of such a study performed on critical CO_2 is presented below.

5.1. Critical behaviour

A fluid close to its critical point is characterised, above (below) T_C, by the existence of fluctuating domains of high (low) density in the gaseous (liquid) phase. These domains, whose average size ξ diverges at the transition,

are responsible for the famous critical opalescence observed in carbon dioxide close to $T_C = 304.1$ K. Indeed, these density fluctuations scatter an incident radiation (visible light, X-rays, neutrons, …) when its wavelength is of the same order of magnitude as the correlation length ξ. The characteristic fluctuations relaxation time τ and the $Q = 0$ static susceptibility χ_0 (macroscopic isothermal compressibility) also diverge upon approaching the transition.

When dealing with a critical system, the relevant scaling parameter is $x = Q\xi$. One can identify two asymptotic regimes: if $Q\xi \ll 1$, neutrons probe over distances much larger than the fluctuation correlation length and one gets information on the hydrodynamic regime; on the other hand, if $Q\xi \gg 1$, neutrons probe the critical regime. Intermediate $Q\xi$ values correspond to a crossover regime [50–52]. The first experimental studies of a critical fluid were performed using light scattering [53]. In this case, due to the typical values of the wavelength ($\lambda \approx 6000$ Å), the modulus of the probed momentum transfer Q is of the order of 10^{-4}–10^{-3} Å^{-1}. It then turns out that light scattering is mainly sensible to the hydrodynamic regime. Due to the much shorter wavelength of neutrons, neutron scattering is the best tool for investigating the different critical, crossover and hydrodynamic regimes; for example with a wavelength of 6 Å, the condition $Q\xi = 100$ is obtained at $T - T_C = 0.40$ K while for light $T - T_C$ should be 10^{-4} K! Moreover, scaling can be easily checked as a same value of $x = Q\xi$ is reached from various ξ and Q combinations.

The dynamic structure factor $S(Q, \omega)$ can be considered as the Fourier transform of the density fluctuation correlation function (and more generally as the Fourier transform of the order parameter correlation function; this formalism can also be applied to magnetic critical phenomena for instance). It is related, via the fluctuation–dissipation theorem, to the imaginary part of the wave vector dependent susceptibility $\chi''(Q, \omega)$:

$$S(Q, \omega) = S_0\big(1 + n(\omega)\big)\chi''(Q, \omega) \tag{11}$$

where

$$n(\omega) = \frac{1}{\exp(\hbar\omega/k_B T) - 1}$$

is the Bose factor and S_0 a constant.

The frequency dependent part is usually factorized out, and the whole expression can be simplified as, due to critical slowing down, energy transfers are small compared to k$_B$T:

$$S(Q, \omega) = \chi(Q)\omega\big(1 + n(\omega)\big)F(Q, \omega) \approx k_B T \chi(Q) F(Q, \omega) \tag{12}$$

where $\chi(Q)$ is the static wave vector dependent susceptibility and $F(Q, \omega)$ the normalized spectral weight function. The relaxation time τ of the critical fluctuations can be identified to the inverse of the characteristic frequency Γ of $F(Q, \omega)$. In the case of a Lorentzian line shape for the spectral weight function, Γ is nothing else but the half width at half maximum.

The experimental characterization of the static and dynamic aspects of the critical behaviour consists in determining the Q and temperature dependences of respectively $\chi(Q)$ and $F(Q, \omega)$. It has to be underlined that a key point for such experiments is the temperature regulation; the gradient along the sample has to be better than 1 mK cm^{-1} and stable during the experiment.

The susceptibility $\chi(Q)$ can be obtained from the energy integrated cross-section

$$\int_{-\infty}^{\infty} \frac{\mathrm{d}^2\sigma}{\mathrm{d}\Omega\,\mathrm{d}\omega}\,\mathrm{d}\omega \approx k_B T \chi(Q) \tag{13}$$

It can be experimentally determined by two axis neutron scattering measurements, and more particularly by small angle neutron scattering (SANS) which is the best suited technique to probe the divergence of the fluctuations correlation length [54–57]. The critical dynamics can be investigated by means of high resolution quasi-elastic neutron scattering techniques such as neutron spin echo (NSE) which directly gives access to the intermediate scattering function $I(Q, t)$, time Fourier transform of $S(Q, \omega)$, and allows to measure relaxation times ranging between a few picoseconds and a hundred nanoseconds [58,59].

In the following we will present results obtained on CO_2 and C_2D_6 illustrating the universality of the critical properties.
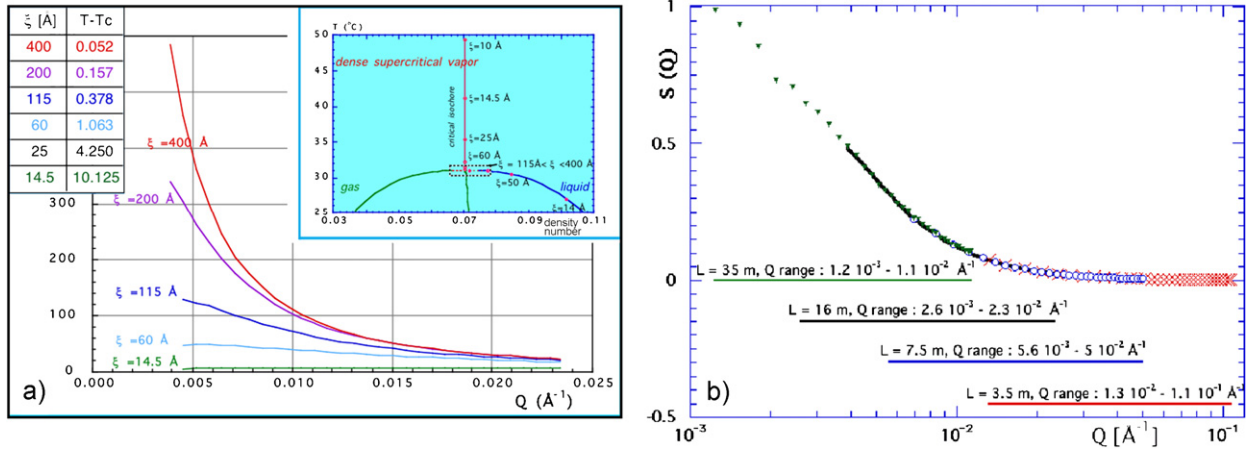
Fig. 9. (a) Divergence of $S(Q)$ recorded on the critical isochore of CO_2 when approaching the critical temperature T_C [$\lambda = 6$ Å on D11, ILL]. The thermodynamic states for which the signals are shown here, are reported on the inset. A precise data analysis leads to the determination of $\xi(T)$ and $\chi(T)$ from Eq. (14) and then to the values of critical exponent γ and ν [54,55]. The regrouping of the different data sets (obtained from several setups on D11 with $\lambda = 6$ Å and 8 Å) as a function of the scaling parameter $x = Q\xi$ gives the experimental static critical scattering function $g(x)$ (from Eq. (15)) in the [0–40] x range [56]. (b) Normalized data for critical scattering at $T - T_C = 0.15$ K using four sample-to-detector distances on D11 ($L = 3.5, 7.5, 16$ and 35 m) ending in an overall Q-range from 1.2×10^{-3} to 1.1×10^{-1} Å^{-1}. The experimental configurations were chosen in such a way that they overlap in a large range. The quality of the regrouping is insured by a precise calibration of the four setups [57]. This run with $\xi = 226$ Å gives access to $g(x)$ from $x = 0.2$ to 22.6.

5.2. Critical statics

The insert of Fig. 9 shows the different fluid states probed by SANS. The following concerns only measurements on the critical isochore. The main graph displays the narrowing of $S(Q)$ at small Q upon approaching the transition temperature. Quantities such as the correlation length ξ and the isothermal compressibility χ_0 are supposed (according to the so-called static scaling hypothesis) to follow power laws of the reduced temperature:

$$\xi = \xi_0 \varepsilon^{-\nu} \quad \text{and} \quad \chi_0 = C\varepsilon^{-\gamma} \quad \text{with } \varepsilon = \frac{T - T_C}{T_C} \tag{14}$$

The Q dependent susceptibility $\chi(Q)$ is the product of χ_0 by an $x = Q\xi$ dependent function $g(x)$ called the universal static scaling function:

$$\chi(Q) = C\varepsilon^{-\gamma} g(Q\xi) \quad \text{with}$$
$$g(x)_{x\to 0} \propto \frac{1}{1+x^2} = g_{OZ}(x) \quad \text{(hydrodynamic regime or Ornstein–Zernike form)}$$
$$g(x)_{x\to\infty} \propto x^{\eta-2} = g_c(x) \quad \text{(critical regime)} \tag{15}$$

The Lorentzian function corresponding to the hydrodynamic regime is often known as the Ornstein–Zernike approximation. The values of the critical exponents γ, ν and η verify a scaling relation ($\gamma = \nu(2 - \eta)$), and depend on the static universality class of the system, which is defined from both the space dimension for the system and the dimension of the order parameter. For instance, CO_2 at the gas–liquid transition belongs to the 3 dimension Ising universality class. $g(x)$ is also supposed to be system independent for a given universality class.

From the SANS data, the values of the static critical exponents γ, ν and η, were determined as well as the $g(x)$ scaling function which was unknown in the intermediate $Q\xi$ domain:

$$\eta = 0.042 \pm 0.006$$
$$\gamma = 1.239 \pm 0.005$$
$$\nu = 0.633 \pm 0.003$$

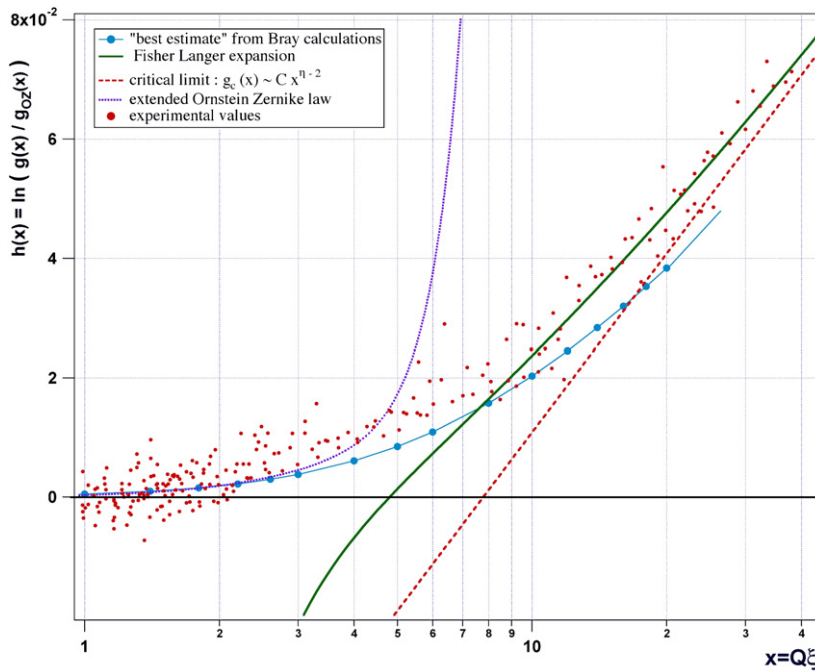These values are in good agreement with those expected for a 3 dimensional Ising system.

Fig. 10. x dependency of $h(x) = \ln(g(x)/g_{OZ}(x))$. The two asymptotic behaviours of the experimental curve (dots) respectively correspond to the hydrodynamic regime where $g(x) \rightarrow g_{OZ}(x)$ for small x values, and to the critical domain where $g(x) \rightarrow g_C(x)$ for large x values. The aim of this representation is to highlight the crossover regime; the experimental data are compared to different models which all fail reproducing the correct x-dependence in the intermediate regime. Reproduced from [56], to which the reader should refer for a detailed presentation of the different models.

For the sake of clarity, Fig. 10 presents the experimentally determined function $h(x)$, logarithm of the ratio of $g(x)$ to the Ornstein–Zernike form $g_{OZ}(x)$. This representation clearly evidences departures from calculated curves based on different models, which all fail reproducing the correct x dependency in the crossover regime.

Before turning to critical dynamics, it is worth mentioning that SANS measurements were also performed on critical water [60]. It was shown that to account for the experimental data, an additional term corresponding to short range correlations between water molecules had to be considered.

5.3. Critical dynamics

Critical dynamics is more complex, as it depends not only on the static universality class but also on conservation laws and equations of motion of the system. The gas–liquid critical point of a pure fluid is treated, theoretically, ignoring sound waves which near T_C, for Q of order ξ^{-1}, are at frequency significantly higher than the diffusive modes (thermal and viscous). This corresponds to model H in the classification of Hohenberg and Halperin [61,62]. Similarly to the static scaling hypothesis assumptions, according to dynamic scaling, the characteristic frequency Γ is supposed to follow

$$\Gamma(Q, \xi) = A Q^z \Omega(x) \tag{16}$$

where $\Omega(x)$ is the dynamical scaling function and z the critical dynamical exponent. z is connected to other critical exponents such as x_λ and x_η, respectively associated to the thermal conductivity λ and to the shear viscosity η_s via the relations $z = 4 - \eta - x_\lambda$ with $x_\lambda + x_\eta = 4 - d + \eta$. According to Kawasaki's model [63], and considering the Ornstein–Zernike approximation for the wave vector dependent susceptibility, one expects:

$$z = 3, \quad A = \frac{k_B T}{16 \eta_S} \quad \text{and} \quad \Omega(x) = \Omega_K(x) = \frac{2}{\pi} \left(x^{-1} + x^{-3} + (1 - x^{-4}) \tan^{-1}(x) \right) \tag{17}$$

From an experimental point of view, when probing the dynamics in the vicinity of T_C for small values of $Q\xi$, one does not only measure critical fluctuations but also hydrodynamic sound waves. The dynamic structure factor $S(Q, \omega)$ is
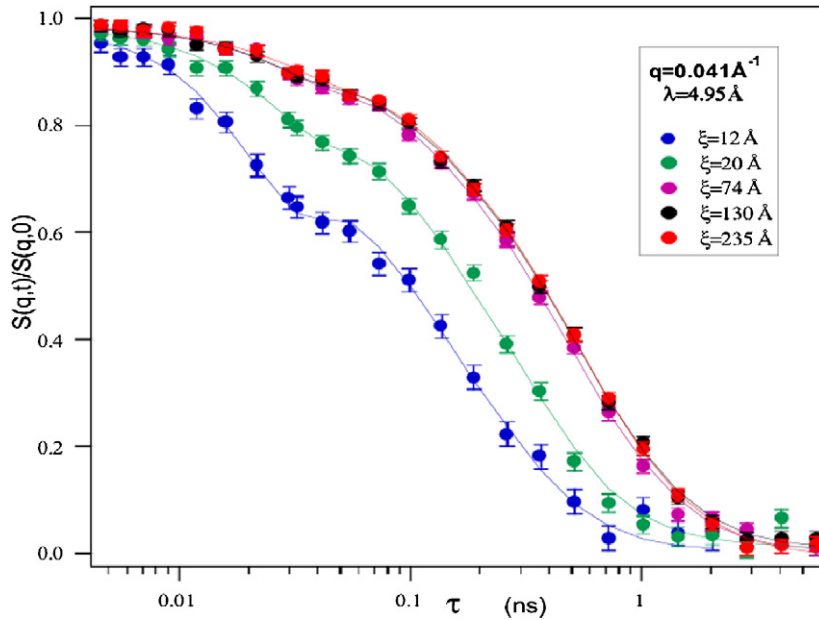
Fig. 11. Critical slowing down as measured on C_2D_6, at $Q = 0.041$ Å^{-1} by NSE [IN11, ILL]. Brillouin component is seen as a sine modulation superimposed on the pure exponential relaxation corresponding to the Rayleigh line; it is mainly visible at small ξ [59].

then the sum of a propagative component, the Brillouin doublet, and a diffusive one, the Rayleigh line, the respective widths of which are $\Gamma_B = D_s Q^2$ and $\Gamma_R = D_T Q^2$

$$S(Q, \omega) = \left(1 - \frac{C_V}{C_P}\right) \frac{2 D_T Q^2}{\omega^2 + (D_T Q^2)^2} + \frac{C_V}{C_P} \left\{ \frac{\frac{1}{2} D_S Q^2}{(\omega - c_s Q)^2 + (\frac{1}{2} D_S Q^2)^2} + \frac{\frac{1}{2} D_S Q^2}{(\omega + c_s Q)^2 + (\frac{1}{2} D_S Q^2)^2} \right\} \quad (18)$$

C_P and C_V are respectively the constant pressure and constant volume heat capacities, c_s is the sound velocity, D_S the sound wave damping constant and D_T the macroscopic coefficient for thermal diffusivity. Upon approaching the critical temperature, the Landau–Placzek ratio of the Rayleigh to Brillouin intensities $I_R / 2 I_B$ diverges and the doublet moves into the quasi-elastic line the width of which narrows. In the critical regime, $S(Q, \omega)$ reduces to a single diffusive mode. On Fig. 11, the critical slowing down is shown by the increase of the relaxation time with ξ. While the relaxation is purely exponential close to the phase transition, a Brillouin component is visible for low ξ values.

The intermediate scattering function corresponding to the above dynamical structure factor, and which was used to analyse the NSE data, is

$$I(Q, t) = I_R \exp(-\Gamma_R t) + I_B \cos(c_s Q t) \exp(-\Gamma_B t) \quad (19)$$

Fig. 12 shows experimental values of $\Gamma_R / A Q^3$ as a function of $1/x$ obtained for both C_2D_6 and CO_2. In the frame of Kawasaki's model, such a plot evidences the universal dynamic function of Eq. (16). The most obvious feature is the confirmation of universality, CO_2 and C_2D_6 data describing a same universal function. Besides that, a clear departure from the Kawasaki's theoretical curve (Eq. (17)) is shown. This is not very surprising. Indeed, one of the limitations of this model is that it does not satisfy the boundary condition imposed by the dynamical scaling hypothesis in the large x limit, as it does not depend on x, instead varying as $x^{x\eta}$. There are different ways of improving this. One consists in taking into account the frequency and wave vector dependence of the viscosity, as done by Burstin [64]. These models could also be improved by the introduction of the static universal scaling function $g(x)$ determined by SANS, instead of considering the crude Lorentzian approximation.

To summarize, the static aspects of the critical behaviour were investigated by SANS for Q values ranging between about 10^{-3} and 10^{-1} Å^{-1} and reduced temperatures spanning from about 5×10^{-5} to 5×10^{-2}. This allowed a precise characterisation of the system from the critical to the hydrodynamic regimes. Dynamics was probed in the Q domain
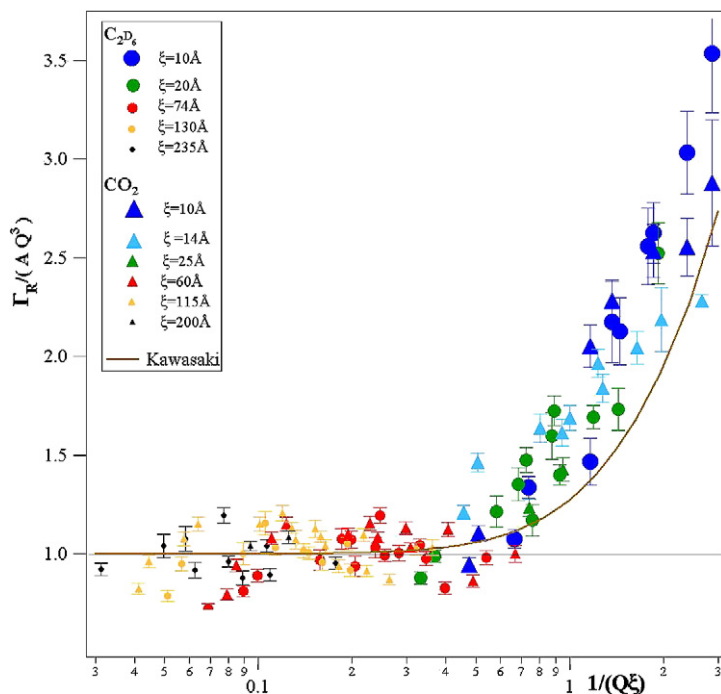
Fig. 12. Experimental universal dynamical function Γ_R/Q^3 as a function of the dimensionless parameter $1/Q\xi$ determined by NSE measurements on CO_2 (triangles) and C_2D_6 (dots), compared to the Kawasaki model (line) [58,59].

2×10^{-2} to 2×10^{-1} Å^{-1}, using NSE which gave access to Fourier times spanning from 5×10^{-2} to 5 ns. Neutron scattering is clearly the ideal tool for probing critical fluids.

6. Structure and dynamics of liquids under confinement

In numerous relevant situations, liquids are not in bulk but instead found filling small cavities. Water trapped in porous media such as rocks or in biological materials is a notorious example of such a 'confined liquid'. But the non-vanishing interest for the structure and dynamics of liquids in restricted geometries is shaped by more than just practical or technological considerations. Confinement, in other words imposing a characteristic size smaller that the 'natural size' of a system, leads to surprisingly rich physical behaviours, usually summarised by thermodynamical phase diagrams significantly modified as compared to the situation in bulk: shift or suppression of phase transitions, stabilisation of usually metastable states [65–67]. Frustration to the growth of correlation or cooperative lengths has, for example, long been thought to be a route to a better understanding of the still highly debated phenomenon of glass transition. Unfortunately, the smaller the confining cavities get, the larger interfacial effects between the confined liquids and the host matrice get too, blurring quite a bit the pure influence of just the confining size, but giving rise to unexpected and intriguing structural and dynamical behaviours.

Here the interplay between volume and surface effects is shown in the case of confined water. We illustrate how neutron scattering techniques, based at reactor or spallation sources, can be taken advantage of, to track down the physics of confined molecular liquids. SANS is used to characterize the large scale structure of the confining material e.g. pore radius and specific surface area. The local atomic structures of the different phases of water induced by confinement—i.e. a purely volume effect—but also by specific interaction with the surface of the confining material, are evidenced by neutron crystallography (coherent elastic neutron scattering). Quasi-elastic neutron scattering is used to address the dynamical behaviour, both translational and rotational, of the confined and interfacial liquid; these measurements show a liquid behaviour for the interfacial water at a temperature as low as 165 K. Incoherent high energy inelastic scattering reveals that such a peculiar dynamical behaviour is due to a significant weakening of the hydrogen-bond strength.
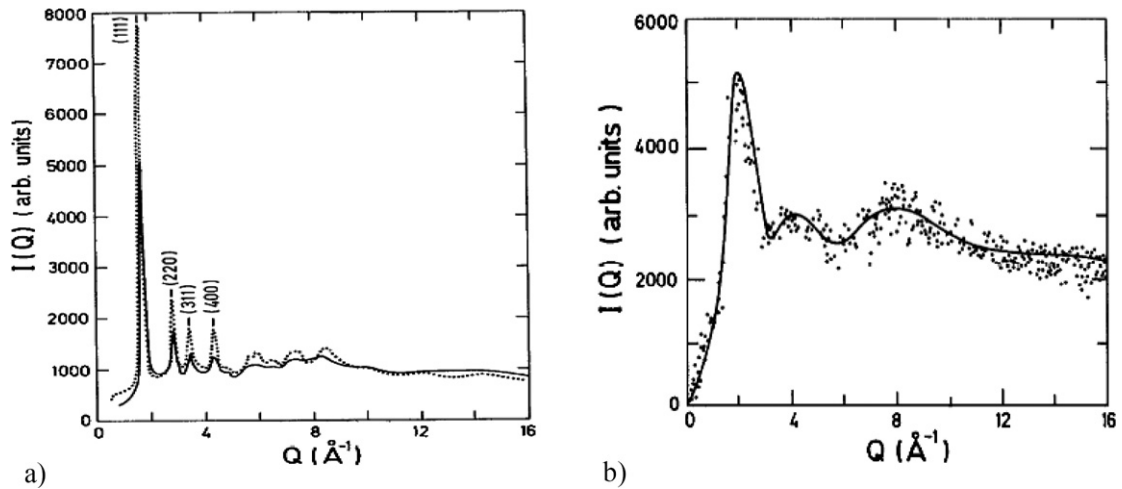
Fig. 13. (a) Spectrum of cubic ice at $-198\,^{\circ}$C (75 K) (dotted line) and confined D_2O in fully hydrated Vycor at $-100\,^{\circ}$C (173 K) (full line). (b) Diffraction pattern (the full line is a guide for the eye) of the small amount ($\approx23\%$ of total water mass) of water still not crystallized (i.e. remaining liquid or amorphous) at $-18\,^{\circ}$C (255 K) in a fully hydrated Vycor where water crystallisation in cubic phase has occurred. Water with a similar structure can be detected down to 233 K. Reproduced from [71].

6.1. SANS: Large scale structure of the porous material

Vycor [68] is a SiO_2 open porous network and has been characterized by SANS. The broad peak centred at $Q_M = 0.02$ Å^{-1} gives a characteristic size of $1/Q_M = 50$ Å. The $(S/m)Q^{-4}$ power law at high Q is the signature of a clear-cut interface where $S/m = 130$ m^2 g^{-1} is the material specific surface area [69,70]. The numerous silanol (Si–OH) groups covering its surface make the Vycor a very hydrophilic material. It can for example easily absorb water up to 25% of its dry mass. Partially hydrated samples can also be prepared by absorption of water in the vapour phase. In this paper, we will specifically consider two extreme samples: (i) fully hydrated Vycor (corresponding to the mass ratio $x_m = m_{\text{water}}/m_{\text{dry Vycor}} = 0.25$); and (ii) low hydrated sample ($x_m = 0.06$ also referred as 25% hydration). In the latter, water realizes monolayer coverage of the Vycor surface and will be referred to, hereafter, as interfacial water.

6.2. Neutron crystallography: local structure of the confined fluid

At room temperature and full hydration, the structure factor of water (here D_2O) confined in Vycor is very similar to that of bulk water. Due to the Gibbs–Thomson effect [65,66], in such deep confinement, water can be supercooled down to $-18\,^{\circ}$C (255 K). At this temperature crystallisation occurs, but instead of freezing in hexagonal ice (i.e. the usual situation in bulk), in this confined geometry water adopts a peculiar structure: cubic ice (Fig. 13(a)). Moreover, it is worthwhile to note, as shown on Fig. 13(b), that careful analysis of the diffraction patterns enables to detect small amounts of non-crystalline water down to $-40\,^{\circ}$C (233 K).

A question then arises: is this non-crystalline water an amorphous solid or a liquid? Below, we show that incoherent inelastic neutron scattering is the perfect tool to tackle such an issue.

6.3. Quasi-elastic neutron scattering: probing diffusive dynamics

Based on incoherent neutron scattering data [72] and subsequent computer molecular dynamics simulations [73], a picture of the short time (picosecond) local bulk water dynamics is available (Fig. 14). If the rotational and translational dynamics at play to describe dynamics of water are supposed uncorrelated, the global dynamics of a single water molecule is:

$$S_{\text{inc}}(Q, \omega) = A_0(Q).L_{\text{trans}}(Q, \omega) + \big(1 - A_0(Q)\big)L_{\text{Trans}}(Q, \omega) \otimes L_{\text{Rot}}(Q, \omega) \tag{20}$$
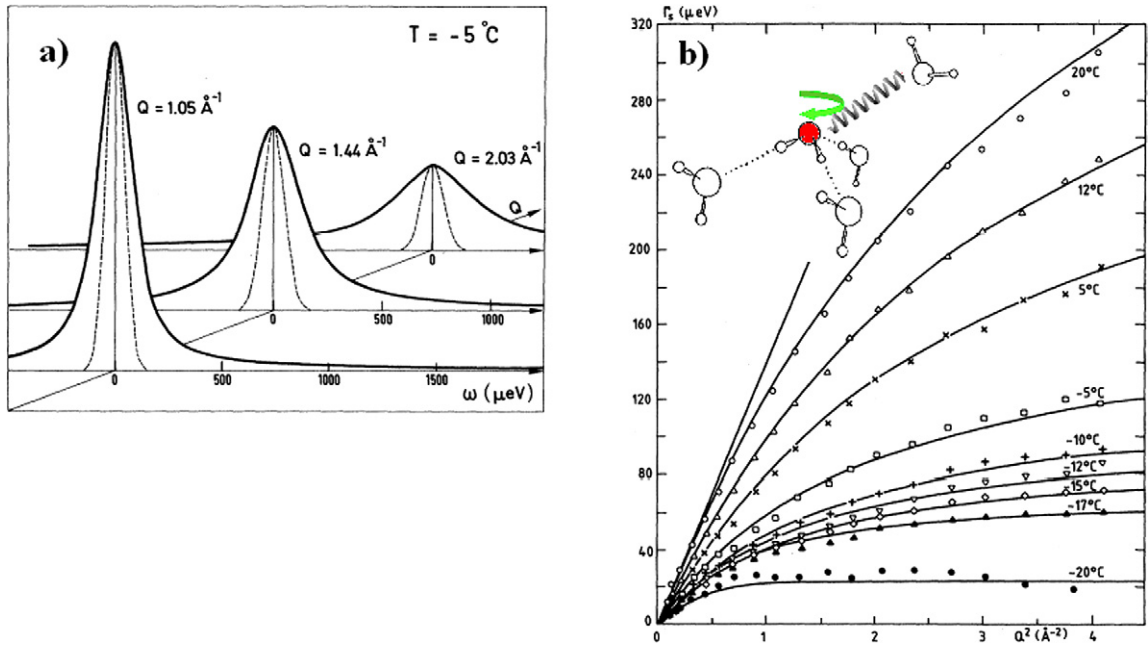
Fig. 14. Incoherent scattering in bulk liquid water. (a) Q dependence of the quasi-elastic signal (full bold line) at $-5\,°C$; the thin lines show the instrumental resolution. The rotational contribution L_{Rot} (see Eq. (20)) is not discernable on this scale. (b) Temperature dependence as a function of Q^2 of Γ (µeV), the HWHM of the quasi-elastic Lorentzian broadening L_{Trans} (Eq. (20)). At small Q, Γ is linear with Q^2 and the translational diffusion coefficient D_t is evaluated from the Fick's law by the slope of the tangent at the origin. Departures from the '$D_t Q^2$ law' are visible at larger Q indicating a jump diffusion mechanism. Reproduced from [72].

L_{Rot} and L_{Trans} stand for Lorenzian lines describing the rotational and translational diffusive motions, respectively. $A_0(Q)$ is the Elastic Incoherent Structure Factor (EISF). As stated in Section 2.1, when dealing with a purely incoherent sample, an inelastic neutron experiment directly probes the self-correlation function. The atoms experiencing a localized dynamic within the sample are somehow 'trapped' in a well defined region of the space and as a consequence, their self-correlation function does not decay to 0. Physically, the EISF is the form factor defined by the loci of the infinite time tail of the intermediate self-correlation function $I_s(Q, t)$, the space Fourier transform of $G_s(r, t)$ introduced Section 2.1. In the case of a water molecule under constant reorientation, the hydrogen atoms experience an isotropic rotation over the intramolecular OH distance, $r_{OH} = 0.98$ Å, and the EISF is

$$A_0(Q) = I_s(Q, t = \infty) = \int \exp[iQr][G_s(r, \infty)]\, dr = [j_0(Qr_{OH})]^2$$

In bulk water, for room temperature down to the deep supercooled regime, the width of the quasi-elastic Lorentzian broadening L_{Trans} is proportional to Q^2 at small Q ($Q < 0.7$ Å^{-1}) i.e. on a large spatial scale (Fig. 14). The slope of Γ versus Q^2, is a direct measurement of the translational diffusion coefficient of the water molecules: $D_t = 2.0 \times 10^{-9}$ m^2 s^{-1} at 20 °C. A departure at larger Q from the Fick's law is clearly visible when one gets sensitive to the detailed molecular motion underlying the macroscopic fluidity of the liquid: jump diffusion between local sites. In bulk liquid water, a molecule is hydrogen bonded to on average slightly less than four neighbouring molecules (see insert of Fig. 14(b)). If due to thermal energy, a hydrogen bond O–H–O moves apart from linearity by more than 25°, the bond breaks. When several H-bonds engaged by a molecule are simultaneously broken, the molecule is free to experience a rotational diffusive motion until several hydrogen bonds are formed again leading to the formation of a transient localization 'site'. The level of the large Q plateau of Γ versus Q^2 (Fig. 14(b)), allows a direct measurement of the residence time in this 'site': 1.2 ps at 20 °C and 22.7 ps at -20 °C. It is important to note that within this mechanism, long range translational dynamics can only occur if rotational dynamics is present.

In interfacial water, when dealing with just a monolayer of water molecules, this mechanism is still at play with an average number of H-bonds per molecule reduced to three. The model defined by Eq. (20) is also suitable to access
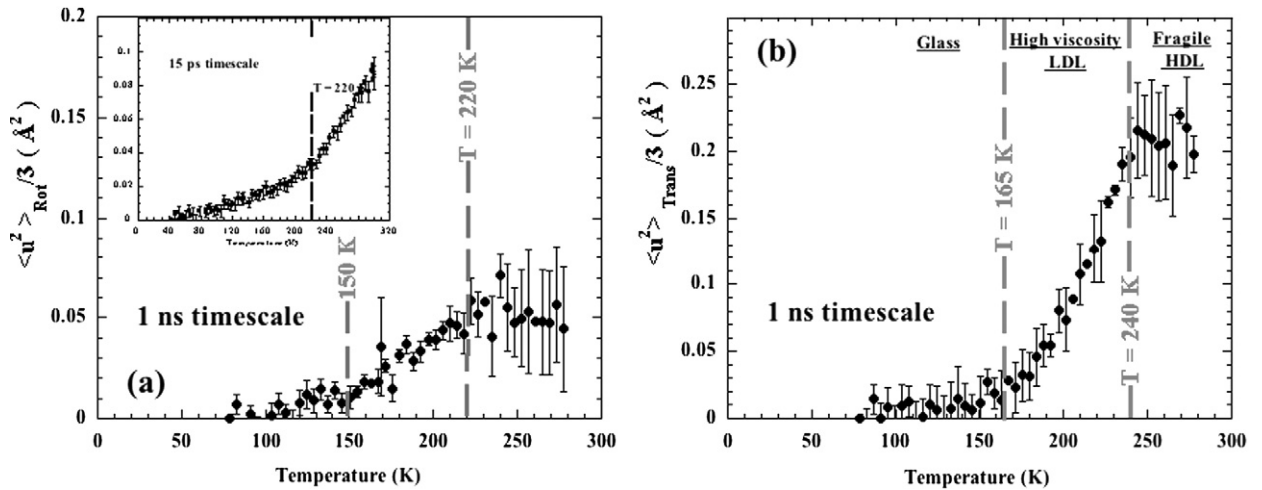
Fig. 15. Temperature dependences of rotational and translational mean-square displacements of interfacial water $\langle u^2 \rangle_{\text{Rot}}$ (a) and $\langle u^2 \rangle_{\text{Trans}}$ (b) (IN16 data, ILL, France). From Eq. (20), it is clear that one can take advantage of the different Q dependences of weighting factors of the translational and rotational contributions to discriminate between them. $\langle u^2 \rangle_{\text{Rot}}$ and $\langle u^2 \rangle_{\text{Trans}}$ have been extracted from two distinct Q ranges ($Q > 1. \text{ Å}^{-1}$ and $Q < 1. \text{ Å}^{-1}$ respectively). The different transitions detected in water, local (high Q) rotational (a) and long range (small Q) translational (b) behaviours, are noted by dashed lines. As expected in water, where translational dynamics is driven by hydrogen bond life-time (i.e. rotational behaviour, see Fig. 14), any transition in the long range translational behaviour is preceded by a transition in the water molecules rotational behaviour. Reproduced from [78].

water dynamics for water confined in Vycor at different levels of hydration [74]: at room temperature, interfacial water at the Vycor hydrophilic surface adopts the behaviour of supercooled water. At all temperatures down to 258 K, we observe a downshift of 30 K in the structural and dynamical properties of the interfacial water with respect to bulk water. Below that temperature, correlation times become too long to be accessed by a full lineshape analysis of the inelastic structure factor $S(Q, \omega)$. Even in such a case, when the instrumental energy resolution is a severe limiting factor to fully assess the detailed sample dynamical behaviour, a way through remains: the elastic scan. Performing an elastic scan means scanning over a wide temperature range, while recording at each temperature the Q dependence of the elastic intensity (Lamb–Mossbauer effect). In a similar way to the Debye–Waller effect, the Q dependent Gaussian intensity loss $\exp(-Q^2.\langle u^2 \rangle)$ can be related to the spatial extension ($\langle u^2 \rangle$) of atoms around their equilibrium position. Using such a strategy, both rotational and translational water mean-square displacements, respectively $\langle u^2 \rangle_{\text{Rot}}$ and $\langle u^2 \rangle_{\text{Trans}}$, can be assessed by detailed analysis of the elastic signal $S(Q, \omega \approx 0)$ Q dependence. These experimental dynamic results are combined with calorimetric, diffraction and quasi-elastic neutron scattering data to show that, after exhibiting a glass transition at 165 K, interfacial water experiences a first order liquid-liquid transition at 240 K from a low density to a high density liquid [75]. The obtained QENS data demonstrate that on a timescale of 1 nanosecond:

(i) $\langle u^2 \rangle_{\text{Rot}}$ significantly increases above 150 K (Fig. 15(a)). This is the onset of rotational dynamics of the water molecules.

(ii) Below 165 K, interfacial water is a low density amorphous (LDA) ice (with $Q_0 = Q_0^{\text{LDA}} = 1.71 \text{ Å}^{-1}$ [75] the first peak in $S(Q)$ structure factor) showing no long range translational dynamics ($\langle u^2 \rangle_{\text{Trans}} \approx 0$, Fig. 15(b)). Above 165 K, no change is observed in water density but translational dynamics becomes possible on a 1 nanosecond timescale, as shown by the $\langle u^2 \rangle_{\text{Trans}}$ non-null value. This is a clear signature of a glass transition at 165 K (Fig. 15(b)).

(iii) At 240 K, this Low Density Liquid (LDL) experiences a transition to High Density Liquid HDL ($Q_0 = 1.86 \text{ Å}^{-1}$) and rotational and translational correlation times related to $\langle u^2 \rangle_{\text{Trans}}$ and $\langle u^2 \rangle_{\text{Rot}}$ significantly decrease leading to a 'saturation' of the signal on IN16 (Fig. 15). An experiment at lower resolution, i.e. shorter timescale (QENS, ANL/IPNS), actually shows that $\langle u^2 \rangle_{\text{Rot}}$ increases (insert Fig. 15) above 220 K, confirming this 'saturation' effect.
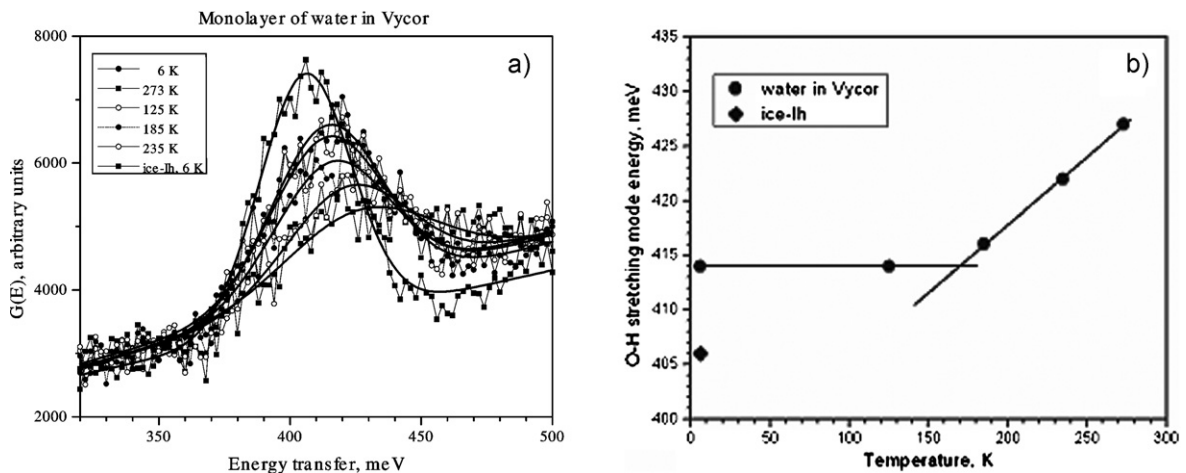
Fig. 16. (a) Vibrational density of states measured with incident neutron energy $E_i = 600$ meV (lines with points) and their Gaussian fit (curves without points) of a water monolayer on Vycor in the range of O–H stretching modes as a function of temperature from 6 to 273 K (HRMECS, ANL/IPNS); dry Vycor spectrum was subtracted. Ice-Ih signal is given for comparison. (b) Temperature dependence of O–H stretching modes (midpoints of the Gaussians) from the spectra in (a). Reproduced from [77].

As a summary, interfacial water is found to experience long range translational motion (i.e. is a liquid) at temperature as low as 165 K. In the next section, we show that spallation source based inelastic neutron scattering can help to elucidate the origin of such an unusual behaviour.

6.4. Deep inelastic neutron scattering: probing the hydrogen bond strength

The intramolecular O–H stretching modes of interfacial water (see Fig. 16) compared to ice I-h at the same temperature (6 K) exhibit a strong shift towards higher energy (406 meV in bulk ice and 414 meV in interfacial water). This energy remains almost unchanged up to $T = 125$ K and it increases approximately linearly with temperature at $T > 170$ K, as clearly seen in Fig. 16(b). As shown by IR study of ice-VII under pressure [76], a shift of the intramolecular O–H stretching modes towards higher energy is expected to be associated with a decrease of the H-bond strength. Thus, the high energy experiment leads to the conclusion that H-bonds in interfacial water at temperatures below 125 K are already weaker than in bulk ice, and at 235 K and above are significantly weaker, being similar to those in bulk liquid water. There is a crossover in the maximum of the peak position of G(E) (Fig. 16(b)) which suggests a phase transition in water at $T \sim 170$ K.

As a conclusion, neutron scattering is a powerful tool to probe the structure and dynamics of liquids under deep confinement. As far as water is concerned, implications of the present results in the field of bulk water physics (existence of a second critical point at low temperature) and protein dynamics are discussed elsewhere [78].

7. Conclusion

As opposed to perfect crystal or perfect gas models, there is no obvious parameter to describe the order or disorder of the liquid state even for simple monoatomic liquids. In liquids the concepts of order and (dynamic) disorder are scale-dependent and driven by various competing interactions. A complete understanding of the liquid state aims to correlate the microscopic description to the macroscopic properties and partial descriptions are scaled upon different characteristic sizes or times. This has been particularly well established for complex polymeric liquids for which the coarse-grained level results in the scaling approach of the theory of polymers [79].

This paper is clearly not an exhaustive overview of the contributions of neutron scattering in the field of the physics of liquids. The examples picked here have mainly been selected to illustrate the various approaches to probe both different time and length scales (independently or concurrently) using neutron scattering. As seen throughout these examples, the palette of the experimental neutron techniques is wide: small angle scattering, diffraction (or diffuse scattering) at large angle, quasi-elastic and inelastic scattering. While the coherent scattering sheds light on the cor-

related fluctuations (including the particle autocorrelation) and collective modes, the incoherent scattering probes the self correlation: vibrational modes, self-diffusion and related characteristic lengths (EISF). Besides the examples given here, we have to mention significant fields of interest:

(i) The usefulness of the isotopic substitution in neutron scattering measurements has been just briefly mentioned in Section 2. It is a key tool to balance between individual (incoherent) and collective (coherent) properties (particularly using H/D substitution) or to separate various contributions in complex systems by varying their contrast. The complete determination of independent partial structure factors has been discussed in detail by Price et al. [80] and numerous examples are given in the review from Fischer et al. [2, references therein]. Let us also mention the recent paper reviewing the structural properties of alkali ions in aqueous solutions as measured by these 'difference methods', NDIS and AXD; furthermore, combination of NDIS techniques with MD simulations allows one to define the local order around complex ions and biological molecules [81].

(ii) During the past decade an important experimental work on 'noble' fluids (Ar [82], Kr [83], Xe [84], Ne [85]) and simple diatomic liquids (N_2 [86], H_2, D_2 [87]) aiming to gain insight on the long range interactions: very precise $S(Q)$ measurements at low Q values allow to study different pair potential models and lead to the detection of three-body effects; quantum effects were discussed in case of liquid hydrogen and deuterium [87].

(iii) Collective dynamics in liquids is also an important field of research, which should strongly develop in the coming years in connexion with the Brillouin scattering devoted instrument which is coming into operation at the ILL (it consists in an inelastic neutron spectrometer at thermal energies optimised for small angle experiments). These studies show different dynamical behaviours, depending on the nature of the liquid. A subject of interest is the collective centre of mass dynamics in molecular liquids, the investigation of which is complicated by the existence of intramolecular dynamics [88]. Strong efforts are also devoted to the dynamics of liquid metals and more particularly to the understanding of the microscopic mechanisms responsible for the propagation and the attenuation of density fluctuations in these systems [89]; last but not least, molten salts provide a potentially rich field for coupling experiments and theory because two classes of fluctuations, density and charge, can be probed by inelastic neutron scattering [90]. For a comprehensive discussion of atomic motion in simple liquids and theoretical approaches developed for the dynamical properties of liquids, the interested reader should refer to the book from Balucani and Zoppi [91] that complements Egelstaff's reference textbook [1].

(iv) Lastly, we would like to underline the benefits for the study of the liquid state of complementary approaches, among which computer simulation techniques, X-ray scattering and spectroscopy, for which some examples have been given here, but also with NMR and more conventional RAMAN and IR spectroscopy.

Current limits of neutron scattering are mostly due to the moderate intensity of neutron beams as compared to the extreme brilliance of synchrotron sources, requiring then relatively large samples or large counting times. With the advent of new spallation sources, these current limits alongside a significant extension of the $Q–\omega$ plane, will be pushed in a decisive way and benefit to an even deeper demystification of the liquid complexity.

References

[1] P.A. Egelstaff, An Introduction to the Liquid State, second ed., Oxford University Press, 1994.
[2] H.E. Fischer, A.C. Barnes, P. Salmon, Rep. Prog. Phys. 69 (2006) 233.
[3] P. Chieux, J. Molecular Struct. 296 (1993) 177.
[4] J.P. Hansen, I.R. McDonald, Theory of Simple Liquids, third ed., Elsevier Academic, London, 2006.
[5] R.L. McGreevy, J. Phys. IV 111 (2003) 347.
[6] D.M. North, J.E. Enderby, P.A. Egelstaff, J. Phys. C: Solid State Phys. 1 (1968) 784.
[7] D.L. Price, M.-L. Saboungi, J. Bermejo, Rep. Prog. Phys. 66 (2003) 407.
[8] T. Scopigno, G. Ruocco, F. Sette, Rev. Mod. Phys. 77 (2005) 881.
[9] W.-C. Pilgrim, J. Neutron Res. 14 (4) (2006) 345.
[10] D. Turnbull, J. Appl. Phys. 21 (1950) 10228.
[11] F.C. Frank, Proc. R. Soc. Lond. A 215 (1952) 436.
[12] P.J. Steinhardt, D.R. Nelson, M. Ronchetti, Phys. Rev. B 28 (1983) 784805.
[13] H. Jonsson, H.C. Andersen, Phys. Rev. Lett. 60 (1988) 22958.
[14] H. Reichert, O. Klein, H. Dosch, M. Denk, V. Honkimaki, T. Lippmann, G. Reiter, Nature 408 (2000) 839.
[15] D.M. Herlach, R.F. Cochrane, I. Egry, H.-J. Fecht, A.L. Greer, Int. Mater. Rev. 38 (1993) 27347.
[16] D. Holland-Moritz, O. Heinen, R. Bellissent, T. Schenk, Mat. Sci. Eng. A 449451 (2007) 4245.

[17] T. Schenk, D. Holland-Moritz, V. Simonet, R. Bellissent, D.M. Herlach, Phys. Rev. Lett. 89 (2002) 75507.
[18] A.F. Ioffe, A.R. Regel, Prog. Semiconduct. 4 (1960) 237.
[19] J.P. Gaspard, A. Pellegati, F. Marinelli, C. Bichara, Phil. Mag. 3 (1998) 727.
[20] Y. Tsuchiya, J. Phys. Soc. Jpn. 60 (1991) 227.
[21] Y. Tsuchiya, H. Saitoh, J. Phys. Soc. Jpn. 62 (1993) 1272.
[22] R.L. McGreevy, L. Pusztai, Mol. Simul. 1 (1988) 359;
     R.L. McGreevy, J. Phys.: Condens. Matter 13 (2001) R877.
[23] M.-V. Coulet, D. Testemale, J.L. Hazemann, J.P. Gaspard, C. Bichara, Phys. Rev. B 72 (2005) 174209.
[24] C. Bergmann, C. Bichara, J.P. Gaspard, Y. Tsuchiya, Phys. Rev. B 67 (2003) 104202.
[25] C. Bichara, M. Jonhson, J.P. Gaspard, Phys. Rev. Lett. 95 (2005) 267801.
[26] G.-F. Zhou, Mat. Sci. Eng. A 304–306 (2001) 3.
[27] A. Kolobov, P. Fons, A. Frenkel, A. Ankudinov, J. Tominaga, T. Uruga, Nature Mater. 3 (2004) 703.
[28] W. Welnic, A. Pamungkas, R. Detemple, C. Steimer, S. Blgel, M. Wuttig, Nature Mater. 5 (2006) 56.
[29] M.V. Coulet, J.P. Gaspard, B. Beuneu, W. Welnick, M. Wuttig, C. Bichara, submitted for publication.
[30] G. Dolling, B.M. Powell, V.F. Sears, Mol. Phys. 37 (1979) 1859.
[31] F. Leclercq, P. Damay, M. Foukani, J. Chem. Phys. 102 (1995) 4400.
[32] P. Damay, F. Leclercq, P. Chieux, Phys. Rev. B 41 (1990) 9676.
[33] F. Leclercq, P. Damay, P. Chieux, J. Phys. IV 1 (C5) (1991) 357.
[34] F. Leclercq, P. Damay, M. Foukani, P. Chieux, M.-C. Bellissent, A. Rassat, Phys. Rev. B 48 (1993) 2748.
[35] P. Damay, F. Leclercq, Phys. Rev. B 49 (1994) 7790.
[36] L. Descotes, Thesis, Orsay, 1994;
     R. Bellissent, L. Descotes, F. Boué, P. Pfeuty, J. Phys. Condens. Matter 6 (1994) A211.
[37] V. Simonet, F. Hippert, H. Klein, M. Audier, R. Bellissent, H. Fischer, A.P. Murani, D. Boursier, Phys. Rev. B 58 (1998) 6273.
[38] M.V. Coulet, C. Bichara, R. Bellissent, J. Phys. Condens. Matter 18 (2006) 116.
[39] M.C. Bellissent-Funel, L. Bosio, J. Teixeira, J. Phys. Condens. Matter 3 (1991) 116.
[40] F. Cavillon, Thesis, Lille, 2004.
[41] J. Neuefeind, P. Chieux, M.D. Zeidler, Mol. Phys. 76 (1992) 143.
[42] S. Longelin, F. Cavillon, A. Idrissi, F. Leclercq-Hugeux, P. Damay, Physica B: Condens. Matter 350 (2004) 79.
[43] R. Bellissent, L. Descotes, F. Boué, P. Pfeuty, Phys. Rev. B 41 (1990) 2135.
[44] S. Longelin, Thesis, Lille, 2004;
     B. Nicolai, private communication (GAMESS-UK ab initio calculation for C_2D_6 hindered rotation).
[45] H. Bertagnoli, I. Waldner, K. Toheide, H. Fischer, Mol. Phys. 94 (1998) 225.
[46] T. Tassaing, M.-C. Bellissent-Funel, B. Guillot, Y. Guissani, Europhys. Lett. 42 (1998) 265.
[47] A. Botti, F. Bruni, M.A. Ricci, A.K. Soper, J. Chem. Phys. 109 (1998) 3180.
[48] T. Tassaing, M.C. Bellissent-Funel, J. Chem. Phys. 113 (2000) 3332.
[49] I.A. Beta, J.C. Li, M.C. Bellissent-Funel, Chem. Phys. 292 (2003) 229.
[50] D. Sette, Critical phenomena, in: G.K.T. Conn, G.N. Fowler (Eds.), Essays in Physics, vol. 5, Academic Press, London, 1973, p. 95.
[51] H.E. Stanley, Introduction to Phase Transitions and Critical Phenomena, Oxford University Press, 1971.
[52] S.K. Ma, in: D. Pines (Ed.), Modern Theory of Critical Phenomena, in: Frontiers in Physics, fifth ed., 1982.
[53] H.L. Swinney, H.Z. Cummins, Phys. Rev. 171 (1968) 252;
     H.L. Swinney, D.L. Henry, Phys. Rev. A 8 (1973) 2586.
[54] P. Damay, F. Leclercq, P. Chieux, J. Chem. Phys. 88 (1984) 3734.
[55] P. Damay, F. Leclercq, P. Chieux, Phys. Rev. B 40 (1989) 4696.
[56] P. Damay, F. Leclercq, R. Magli, N. Formisano, P. Lindner, Phys. Rev. B 58 (1998) 1203.
[57] P.L. Lindner, F. Leclercq, P. Damay, Physica B 291 (2000) 152.
[58] F. Leclercq, S. Pouget, P. Damay, Neutron spin echo spectroscopy, in: Lecture Notes in Phys., vol. 601, Springer-Verlag, Berlin, 2002, p. 232.
[59] S. Pouget, F. Leclercq-Hugeux, S. Longelin, P. Damay, Physica B: Condens. Matter 350 (2004) 359.
[60] M. Bonetti, G. Romet-Lemonne, P. Calmettes, M.C. Bellissent-Funel, J. Chem. Phys. 112 (2000) 268.
[61] B.I. Halperin, P.C. Hohenberg, Phys. Rev. 177 (1969) 952;
     B.I. Halperin, P.C. Hohenberg, Phys. Rev. 188 (1969) 898.
[62] P.C. Hohenberg, B.I. Halperin, Rev. Modern Phys. 49 (1977) 435.
[63] K. Kawasaki, Phys. Lett. 30A (1969) 325;
     See also K. Kawasaki, Phase Transitions and Critical Phenomena, Academic Press, 1976 (Chapter IV).
[64] H.C. Burstyn, J.V. Sengers, J.K. Bhattacharjee, R.A. Ferell, Phys. Rev. A 28 (1983) 1567.
[65] M. Alcoutlabi, G.B. McKenna, J. Phys.: Condens. Matter 17 (2005) R461.
[66] C. Alba-Simionesco, B. Coasne, G. Dosseh, G. Dudziak, K.E. Gubbins, R. Radhakrishnan, M. Sliwinska-Bartkowiak, J. Phys.: Condens. Matter 18 (2006) R15.
[67] D. Morineau, Surfaces, Interfaces et Milieux confinés par diffusion de Neutrons, in: Collection de la SFN, vol. 8, EDP Sciences, 2007, p. 141.
[68] Vycor brand porous glass n° 7930 is a product of Corning Glass Works.
[69] P. Levitz, G. Ehret, S.K. Sinha, J.M. Drake, J. Chem. Phys. 95 (1991) 6151.
[70] R. Pellencq, B. Rousseau, P. Levitz, Phys. Chem. Chem. Phys. 3 (2001) 1207.
[71] M.-C. Bellissent-Funel, J. Lal, L. Bosio, J. Chem. Phys. 98 (1993) 4246.

[72] J. Teixeira, M.-C. Bellissent-Funel, S.-H. Chen, J. Dianoux, Phys. Rev. A 31 (1985) 1913.
[73] R.W. Impey, P.A. Madden, I.R. McDonald, Mol. Phys. 46 (1982) 513.
[74] J.-M. Zanotti, M.-C. Bellissent-Funel, S.-H. Chen, Phys. Rev. E 59 (1999) 3084.
[75] J.-M. Zanotti, M.-C. Bellissent-Funel, S.-H. Chen, Europhys. Lett. 71 (2005) 91.
[76] D.D. Klug, E. Whalley, J. Chem. Phys. 81 (1984) 1220.
[77] J.-M. Zanotti, M.-C. Bellissent-Funel, S.-H. Chen, A.I. Kolesnikov, J. Phys.: Condens. Matter 18 (2006) S2299.
[78] J.-M. Zanotti, M.C. Bellissent-Funel, A.I. Kolesnikov, Eur. Phys. J. Special Topics 141 (2007) 227.
[79] P.-G. De Gennes, Scaling Concepts in Polymer Physics, Cornell University Press, New York, 1985.
[80] D.L. Price, A. Pasquarello, Phys. Rev. B 59 (1999) 5.
[81] S. Ansell, A.C. Barnes, P.E. Mason, G.W. Neilson, S. Ramos, Ion Hydration Special Issue, Biophys. Chem. 124 (2006) 171.
[82] R. Magli, F. Barocchi, P. Chieux, R. Fontana, Phys. Rev. Lett. 77 (1996) 846.
[83] E. Guarini, G. Casanova, U. Bafile, F. Barocchi, Phys. Rev. E 60 (1999) 6682;
     R. Magli, F. Barocchi, G. Casanova, E. Guarini, M. Tau, Physica B 276–278 (2000) 450.
[84] F. Formisano, F. Barocchi, R. Magli, Phys. Rev. E 58 (1998) 2648.
[85] M. Neumann, M. Zoppi, Phys. Rev. E 65 (2002);
     M. Celli, D. Colognesi, M. Zoppi, A.J. Ramirez-Cuesta, J. Low Temp. Phys. 138 (2005) 887.
[86] F. Barocchi, M.-C. Bellissent Funel, P. Chieux, R. Magli, Physica B 213–214 (1995) 468.
[87] M. Zoppi, J. Phys.: Condens. Matter 15 (2003) R1047;
     M. Zoppi, U. Bafile, M. Celli, G.J. Cuello, F. Formisano, E. Guarini, R. Magli, M. Neumann, J. Phys.: Condens. Matter 15 (2003) S107.
[88] U. Bafile, F. Barocchi, F. Demmel, F. Formisano, E. Guarini, M. Sampoli, G. Venturi, J. Neutron Res. 14 (2006) 284.
[89] F.J. Bermejo, M.L. Saboungi, D.L. Price, M. Alvarez, B. Roessli, C. Cabrillo, A. Ivanov, Phys. Rev. Lett. 85 (2000) 106.
[90] L.E. Bove, F. Formisano, F. Sacchetti, C. Petrillo, A. Ivanov, B. Dorner, F. Barocchi, Phys. Rev. B 71 (2005) 014207.
[91] U. Balucani, M. Zoppi, Dynamics of the Liquid State, Oxford Series on Neutron Scattering, vol. 10, Oxford University Press, 1995.